

Superconductivity and Magnetism in Non-centrosymmetric System: Application to CePt₃Si

Youichi YANASE^{1,2*} and Manfred SIGRIST^{2,3}

¹ Department of Physics, University of Tokyo, Tokyo 113-0033, Japan

² Theoretische Physik, ETH-Honggerberg, 8093 Zurich, Switzerland

³ Department of Physics, Kyoto University, Kyoto 606-8502, Japan

(Received Today 2008)

Superconductivity and magnetism in the non-centrosymmetric heavy fermion compound CePt₃Si and related materials are theoretically investigated. On the basis of the random phase approximation (RPA) analysis of the extended Hubbard model, we describe the helical spin fluctuation induced by the Rashba-type anti-symmetric spin-orbit coupling and identify two stable superconducting phases with either the dominant p -wave ($s+P$ -wave) symmetry or the d -wave ($p+D+f$ -wave) symmetry. The effect of the coexistent antiferromagnetic order is investigated in both states. The superconducting order parameter, quasiparticle density of state, NMR $1/T_1T$, specific heat, anisotropy of H_{c2} , and possible multiple phase transitions are discussed in detail. A comparison with experimental results indicates that the $s+P$ -wave superconducting state is likely realized in CePt₃Si.

KEYWORDS: superconductivity without inversion center, anti-ferromagnetic superconductor, helical spin fluctuation

1. Introduction

The discovery of superconductivity in materials without an inversion center^{1,2} has initiated intensive research on a new aspect of unconventional superconductivity. Several new non-centrosymmetric superconductors with unique properties have been identified among heavy fermion systems such as CePt₃Si,^{1,2} UIr,³ CeRhSi₃,^{4,5} CeIrSi₃,^{6,7} CeCoGe₃⁸ and others like Li₂Pd_xPt_{3-x}B,⁹ Y₂C₃,¹⁰ Rh₂Ga₉, Ir₂Ga₉,¹¹ Mg₁₀Ir₁₉B₁₆,^{12,13} Re₃W,¹⁴ boron-doped SiC¹⁵ and some organic materials.¹⁶

One immediate consequence of non-centrosymmetry is the necessity for a revised classification scheme of Cooper pairing states, as parity is not available as a distinguishing symmetry. Superconducting (SC) states are considered as a mixture of pairing states with different parities or, equivalently, the spin configuration is composed of both a singlet component and a triplet component. The mixing of spin singlet and spin triplet pairings is induced by the anti-symmetric spin-orbit coupling (ASOC).¹⁷ Recent theoretical studies led to the discussion of interesting properties of a non-centrosymmetric superconductor, such as the magnetoelectric effect,¹⁸⁻²¹ anisotropic spin susceptibility^{17,21-29} accompanied by the anomalous paramagnetic depairing effect,²⁹ anomalous coherence factor in NMR $1/T_1T$,^{20,30} anisotropic SC gap,^{28,30-33} helical SC phase,^{29,34-39} Fulde-Ferrel-Larkin-Ovchinnikov (FFLO) state at zero magnetic field,⁴⁰ various impurity effects,⁴¹⁻⁴⁴ vortex state,^{45,46} and tunneling/Josephson effect.⁴⁷⁻⁵²

Non-centrosymmetric heavy fermion superconductors, i.e., CePt₃Si, UIr, CeRhSi₃, CeIrSi₃, and CeCoGe₃, are of particular interests because non- s -wave superconductivity is realized owing to strong electron correlation effects and magnetism has an important effect on the superconducting phase. However, the relation between

magnetism and superconductivity has not been theoretically studied so far, except in studies refs. 28, 53, and 54. Here, we extend our previous study²⁸ and investigate the pairing state arising from magnetic fluctuation in detail.

Another aim of this study is to elucidate the effects of antiferromagnetic (AFM) order on the SC phase. Interestingly, all presently known non-centrosymmetric heavy fermion superconductors coexist with magnetism. We have shown that some unique properties of CePt₃Si at ambient pressure can be induced by the AFM order.^{28,29} In this study, we analyze this issue in more detail.

Among non-centrosymmetric heavy fermion superconductors, CePt₃Si has been investigated most extensively because its superconductivity occurs at ambient pressure,¹ others superconduct only under substantial pressure. Therefore, we focus here on CePt₃Si. We believe that some of our results are qualitatively valid for other compounds too. In CePt₃Si, superconductivity with $T_c \sim 0.5$ K appears in the AFM state with a Néel temperature $T_N = 2.2$ K.¹ The AFM order microscopically coexists with superconductivity.^{55,56} Neutron scattering measurements characterize the AFM order with an ordering wave vector $\vec{Q} = (0, 0, \pi)$ and magnetic moments in the ab -plane of a tetragonal crystal lattice.⁵⁷ The AFM order is suppressed by pressure and vanishes at a critical pressure $P_c \sim 0.6$ GPa. Superconductivity is more robust against pressure and therefore a purely SC phase is present above the critical pressure $P > 0.6$ GPa.⁵⁸⁻⁶⁰

The nature of the SC phase has been clarified by several experiments. The low-temperature properties of thermal conductivity,⁶¹ superfluid density,⁶² specific heat,⁶³ and NMR $1/T_1T$ ⁶⁴ indicate line nodes in the gap. The upper critical field $H_{c2} \sim 3 - 4$ T exceeds the standard paramagnetic limit,¹ which seems to be consistent with the Knight shift data displaying no decrease in spin susceptibility below T_c for any field direction.^{65,66} The

combination of these features is incompatible with the usual pairing states such as the s -wave, p -wave, or d -wave state, and calls for an extension of the standard working scheme.

In ref. 29, we have investigated the magnetic properties of non-centrosymmetric superconductors. Then, it was shown that the predominantly p -wave state admixed with the s -wave order parameter ($s+P$ -wave state) is consistent with the paramagnetic properties of CePt₃Si. We here examine the symmetry of superconductivity in CePt₃Si from the microscopic point of view and show that the $s+P$ -wave state or $p+D+f$ -wave state can be stabilized by spin fluctuation with helical anisotropy. We also calculate the quasiparticle excitations, specific heat, and NMR $1/T_1T$, and show that the line node behavior in CePt₃Si at ambient pressure is consistent with the $s+P$ -wave state. We investigate the pressure dependence of these quantities, possible SC multiple phase transitions, and the anisotropy of H_{c2} . Some future experimental tests are proposed.

The paper is organized as follows. In §2, we formulate the RPA theory in the Hubbard model with ASOC and AFM order. The nature of spin fluctuation and superconductivity is investigated in §3 and §4, respectively. The symmetry of superconductivity, SC gap structure, specific heat and NMR $1/T_1T$, multiple SC phase transitions, and anisotropy of H_{c2} are discussed in §4.1, §4.2, §4.3, §4.4 and §4.5, respectively. Some future experiments are proposed in §4. The summary and discussions are given in §5. A derivation of ASOC in the periodical Anderson model and Hubbard model is given in Appendix.

2. Formulation

2.1 Hubbard model with ASOC and AFM order

For the following study of superconductivity in CePt₃Si, we introduce the single-orbital Hubbard model including the AFM order and ASOC

$$H = \sum_{k,s} \varepsilon(\vec{k}) c_{k,s}^\dagger c_{k,s} + \alpha \sum_k \vec{g}(\vec{k}) \cdot \vec{S}(\vec{k}) - \sum_k \vec{h}_Q \cdot \vec{S}_Q(\vec{k}) + U \sum_i n_{i,\uparrow} n_{i,\downarrow}, \quad (1)$$

where $\vec{S}(\vec{k}) = \sum_{s,s'} \vec{\sigma}_{ss'} c_{k,s}^\dagger c_{k,s'}$ and $\vec{S}_Q(\vec{k}) = \sum_{s,s'} \vec{\sigma}_{ss'} c_{k+\vec{Q},s}^\dagger c_{k,s'}$ with $\vec{\sigma}_{ss'}$ being the vector representation of the Pauli matrix. $n_{i,s}$ is the electron number at the site i with the spin s . We do not touch the heavy Fermion aspect, i.e., the hybridization of conduction electrons with Ce $4f$ -electrons forming strongly renormalized quasiparticles. However, we consider the Hubbard model as a valid effective model for describing low-energy quasiparticles in the Fermi liquid state.⁶⁷

We consider a simple tetragonal lattice and assume the dispersion relation as

$$\begin{aligned} \varepsilon(\vec{k}) = & 2t_1(\cos k_x + \cos k_y) + 4t_2 \cos k_x \cos k_y \\ & + 2t_3(\cos 2k_x + \cos 2k_y) + [2t_4 + 4t_5(\cos k_x + \cos k_y) \\ & + 4t_6(\cos 2k_x + \cos 2k_y)] \cos k_z + 2t_7 \cos 2k_z - \mu, \end{aligned} \quad (2)$$

where the chemical potential μ is included. We

determine the chemical potential μ so that the electron density per site is n . By choosing the parameters as $(t_1, t_2, t_3, t_4, t_5, t_6, t_7, n) = (1, -0.15, -0.5, -0.3, -0.1, -0.09, -0.2, 1.75)$, the dispersion relation eq. (2) reproduces the β -band of CePt₃Si, which has been reported by band structure calculation without the AFM order.^{68–70} The Fermi surface of this tight-binding model is depicted in Fig. 1 of ref. 28. We assume that the superconductivity in CePt₃Si is mainly induced by the β -band because the β -band has a substantial Ce $4f$ -electron character⁶⁸ and the largest density of states (DOS), namely 70% of the total DOS.⁶⁹

The second term in eq. (1) describes the ASOC that arises from the lack of inversion symmetry and is characterized by the vector $\vec{g}(\vec{k})$. Time reversal symmetry is preserved, if the g -vector is odd in \vec{k} , i.e., $\vec{g}(-\vec{k}) = -\vec{g}(\vec{k})$. In the case of CePt₃Si as well as of CeRhSi₃ and CeIrSi₃, the g -vector has the Rashba type structure.⁷¹ The microscopic derivation of the ASOC in the f -electron systems is given in Appendix. The ASOC in the periodic Anderson model as well as that in the Hubbard model originate from the combination of the atomic L - S coupling in the f -orbital and the hybridization with conduction electrons. Although the detailed momentum dependence of the g -vector is complicated (see eq. (A.25)) and is difficult to obtain by band structure calculations, at least from a symmetry point of view, $\vec{g}(\vec{k}) = (-v_y(\vec{k}), v_x(\vec{k}), 0)/\bar{v}$ delivers a reasonable approximation, where $v_{x,y}(\vec{k}) = \partial \varepsilon(\vec{k}) / \partial k_{x,y}$ is the quasiparticle velocity. We normalize $\vec{g}(\vec{k})$ by the average velocity \bar{v} [$\bar{v}^2 = \frac{1}{N} \sum_k v_x(\vec{k})^2 + v_y(\vec{k})^2$] so that the coupling constant α has the dimension of energy. This form reproduces the symmetry and periodicity of the Rashba-type g -vector within the Brillouin zone. We choose the coupling constant $\alpha = 0.3$ in the main part of this paper so that the band splitting due to ASOC is consistent with the band structure calculations.⁶⁹

The AFM order enters in our model through the staggered field \vec{h}_Q without discussing its microscopic origin. The phase diagram under pressure implies that the AFM order mainly arises from localized Ce $4f$ -electrons that have a character different from that of SC quasiparticles. The T_c of superconductivity is slightly affected by the AFM order which vanishes at $P \sim 0.6$ GPa,^{58–60} in contrast to the other Ce-based superconductors.⁷² The experimentally determined AFM order corresponds to $\vec{h}_Q = h_Q \hat{x}$ pointing in the $[100]$ direction with a wave vector $\vec{Q} = (0, 0, \pi)$.⁵⁷ For the magnitude, we choose $|h_Q| \ll W$ where W is the bandwidth since the observed AFM moment $\sim 0.16 \mu_B$ is considerably less than the full moment of the $5/2$ manifold in the Ce ion.⁵⁷

The undressed Green functions for $U = 0$ are represented by the matrix form $\hat{G}(\vec{k}, i\omega_n) = (i\omega_n \hat{1} - \hat{H}(\vec{k}))^{-1}$, where

$$\hat{G}(\vec{k}, i\omega_n) = \begin{pmatrix} \hat{G}^1(\vec{k}, i\omega_n) & \hat{G}^2(\vec{k}, i\omega_n) \\ \hat{G}^2(\vec{k}_+, i\omega_n) & \hat{G}^1(\vec{k}_+, i\omega_n) \end{pmatrix}, \quad (3)$$

and

$$\hat{H}(\vec{k}) = \begin{pmatrix} \hat{e}(\vec{k}) & -h_Q \hat{\sigma}^{(x)} \\ -h_Q \hat{\sigma}^{(x)} & \hat{e}(\vec{k}_+) \end{pmatrix}, \quad (4)$$

with $\hat{e}(\vec{k}) = \varepsilon(\vec{k})\hat{\sigma}^{(0)} + \alpha\vec{g}(\vec{k})\vec{\sigma}$ and $\vec{k}_+ = \vec{k} + \vec{Q}$. The normal and anomalous Green functions $\hat{G}^i(\vec{k}, i\omega_n)$ are the 2×2 matrix in spin space, where $\omega_n = (2n+1)\pi T$ and T is the temperature.

2.2 Éliashberg equation

We turn to the SC instability that we assume to arise through electron-electron interaction incorporated in the effective on-site repulsion U . The linearized Éliashberg equation is obtained by the standard procedure:

$$\lambda \Delta_{p,s_1,s_2}(\vec{k}) = - \sum_{\vec{k}', q, s_3, s_4} V_{p,q,s_1,s_2,s_3,s_4}(\vec{k}, \vec{k}') \psi_{q,s_3,s_4}(\vec{k}'), \quad (5)$$

$$\psi_{p,s_1,s_2}(\vec{k}) = \sum_{i,j,s_3,s_4} \phi_{p,i,j,s_1,s_3,s_2,s_4}(\vec{k}) \Delta_{q,s_3,s_4}(\vec{k}''), \quad (6)$$

where $q = p$ ($q = 3-p$) for $i = j$ ($i \neq j$), $\vec{k}'' = \vec{k} + (i-1)\vec{Q}$ and

$$\phi_{p,i,j,s_1,s_2,s_3,s_4}(\vec{k}) = T \sum_n G_{s_1,s_2}^i(\vec{k}, i\omega_n) \times G_{s_3,s_4}^j(-\vec{k} + (p-1)\vec{Q}, -i\omega_n) \quad (p = 1, 2). \quad (7)$$

Here, we adopt the so-called weak coupling theory of superconductivity and ignore self-energy corrections and the frequency dependence of effective interaction.^{67,73} This simplification strongly affects the resulting transition temperature but hardly affects the symmetry of pairing.⁶⁷ We denote the order parameter for the superconductivity as $\Delta_{p,s_1,s_2}(\vec{k})$ ($p = 1, 2$, s_1 and s_2 are the spin indices), where $\Delta_{1,s_1,s_2}(\vec{k})$ and $\Delta_{2,s_1,s_2}(\vec{k})$ describe the Cooper pairing with the total momenta $(0, 0, 0)$ and $(0, 0, \pi)$, respectively. The former is the order parameter for ordinary Cooper pairs, while the latter is that for π -singlet and π -triplet pairs. These π -pairs are admixed with usual Cooper pairs in the presence of the AFM order.⁷⁴

The effective interaction $V_{p,q,s_1,s_2,s_3,s_4}(\vec{k}, \vec{k}')$ originates from spin fluctuations that we describe within the RPA⁷³ according to the diagrammatic expression shown in Fig. 1. In the RPA, the effective interaction is described by the generalized susceptibility whose matrix form is expressed as

$$\begin{pmatrix} \hat{\chi}_1(\vec{q}) \\ \hat{\chi}_2(\vec{q}_+) \end{pmatrix} = \begin{pmatrix} \hat{1} - \hat{\chi}_1^{(0)}(\vec{q})\hat{U} & -\hat{\chi}_2^{(0)}(\vec{q})\hat{U} \\ -\hat{\chi}_2^{(0)}(\vec{q}_+)\hat{U} & \hat{1} - \hat{\chi}_1^{(0)}(\vec{q}_+)\hat{U} \end{pmatrix}^{-1} \begin{pmatrix} \hat{\chi}_1^{(0)}(\vec{q}) \\ \hat{\chi}_2^{(0)}(\vec{q}_+) \end{pmatrix}, \quad (8)$$

where $\vec{q}_+ = \vec{q} + \vec{Q}$. Hereafter, we denote the element of the 4×4 matrix, such as $\hat{A} = \hat{\chi}_i^{(0)}(\vec{q})$ and $\hat{\chi}_i(\vec{q})$ using the

spin indices as

$$\hat{A} = \begin{pmatrix} A_{\uparrow\uparrow\uparrow\uparrow} & A_{\uparrow\uparrow\uparrow\downarrow} & A_{\uparrow\uparrow\downarrow\uparrow} & A_{\uparrow\uparrow\downarrow\downarrow} \\ A_{\uparrow\downarrow\uparrow\uparrow} & A_{\uparrow\downarrow\uparrow\downarrow} & A_{\uparrow\downarrow\downarrow\uparrow} & A_{\uparrow\downarrow\downarrow\downarrow} \\ A_{\downarrow\uparrow\uparrow\uparrow} & A_{\downarrow\uparrow\uparrow\downarrow} & A_{\downarrow\uparrow\downarrow\uparrow} & A_{\downarrow\uparrow\downarrow\downarrow} \\ A_{\downarrow\downarrow\uparrow\uparrow} & A_{\downarrow\downarrow\uparrow\downarrow} & A_{\downarrow\downarrow\downarrow\uparrow} & A_{\downarrow\downarrow\downarrow\downarrow} \end{pmatrix}. \quad (9)$$

The matrix element of the bare susceptibility $\hat{\chi}_i^{(0)}(\vec{q})$ is expressed as

$$\chi_{1,s_1,s_2,s_3,s_4}^{(0)}(\vec{q}) = -T \sum_{\vec{k}, \omega_n} [G_{s_4,s_1}^1(\vec{k} + \vec{q}, i\omega_n) G_{s_2,s_3}^1(\vec{k}, i\omega_n) + G_{s_4,s_1}^2(\vec{k} + \vec{q}, i\omega_n) G_{s_2,s_3}^2(\vec{k} + \vec{Q}, i\omega_n)], \quad (10)$$

$$\chi_{2,s_1,s_2,s_3,s_4}^{(0)}(\vec{q}) = -T \sum_{\vec{k}, \omega_n} [G_{s_4,s_1}^1(\vec{k} + \vec{q}, i\omega_n) G_{s_2,s_3}^2(\vec{k}, i\omega_n) + G_{s_4,s_1}^2(\vec{k} + \vec{q}, i\omega_n) G_{s_2,s_3}^1(\vec{k} + \vec{Q}, i\omega_n)], \quad (11)$$

and the matrix \hat{U} is obtained as

$$\hat{U} = \begin{pmatrix} 0 & 0 & 0 & -U \\ 0 & 0 & U & 0 \\ 0 & U & 0 & 0 \\ -U & 0 & 0 & 0 \end{pmatrix}. \quad (12)$$

According to Fig. 1, the effective interaction is obtained as

$$V_{1,1,s_1,s_2,s_3,s_4}(\vec{k}, \vec{k}') = V_{2,2,s_1,s_2,s_3,s_4}(\vec{k}, \vec{k}') = -[\hat{U}'\hat{\chi}_1(\vec{k}' - \vec{k})\hat{U}']_{s_3,s_1,s_4,s_2} + \hat{U}_{s_1,s_2,s_3,s_4}, \quad (13)$$

$$V_{1,2,s_1,s_2,s_3,s_4}(\vec{k}, \vec{k}') = V_{2,1,s_1,s_2,s_3,s_4}(\vec{k}, \vec{k}') = -[\hat{U}'\hat{\chi}_2(\vec{k}' - \vec{k})\hat{U}']_{s_3,s_1,s_4,s_2}, \quad (14)$$

where

$$\hat{U}' = \begin{pmatrix} 0 & 0 & 0 & -U \\ 0 & U & 0 & 0 \\ 0 & 0 & U & 0 \\ -U & 0 & 0 & 0 \end{pmatrix}. \quad (15)$$

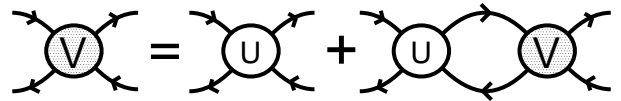


Fig. 1. Diagrammatic representation of the pairing interaction $V_{p,q,s_1,s_2,s_3,s_4}(\vec{k}, \vec{k}')$. The white circle represents the on-site interaction U .

The linearized Éliashberg equation (eqs. (5)-(7)) allows us to determine the form of the leading pairing instability, which is attained for the temperature at which the largest eigenvalue λ reaches unity. Numerical accuracy requires, however, a different but equivalent approach. We perform the calculation at a given temperature, in our case $T = 0.02$, which is much lower than the Fermi temperature, and determine the most stable pairing state

as the eigenfunction of the largest eigenvalue.⁶⁷ The typical eigenvalue at $T = 0.02$ and $U = 4$ lies at around $\lambda = 0.3 \sim 0.6$. This means that the T_c for $U = 4$ is lower than $T = 0.02$. However, the absolute value of T_c is not important for our purpose, which is focused on the roles of the spin fluctuation, ASOC, and AFM order. We believe that the qualitative roles of these aspects can be captured in this simple calculation. On the other hand, the absolute value of T_c is significantly affected by the mode coupling effect, vertex corrections, strong coupling effect, and multi-orbital effect, which are neglected in our calculation. We leave more sophisticated calculation based on the multi-orbital model and beyond the RPA for future discussion.

The T_c of superconductivity reaches $T_c = 0.02$ if we assume a larger U . However, we show the results for $U = 4$, unless stated otherwise. This is mainly because the results for a large U are likely spurious because of the limitation of RPA. Since the mode coupling effect is neglected in the RPA, the critical fluctuation is not taken into account and therefore the magnetic instability is seriously overestimated. When we assume a large U so that we obtain a high T_c , the system approaches the magnetic instability, which is beyond the applicability of RPA. Our results for the superconductivity are only weakly dependent on U except for the relative stability between the $s+P$ -wave and $p+D+f$ -wave states, and therefore we qualitatively obtain the same results for a larger U . However, we avoid parameters close to the magnetic instability.

Note that we here consider the spin fluctuation arising from quasiparticles that are mainly superconducting and may be different from the main source of the AFM moment. Although the quantum critical point of the AFM order exists at $P \sim 0.6$ GPa, the critical fluctuation of the AFM moment slightly affects the T_c of superconductivity, as indicated by the phase diagram in the P - T plane.^{58–60} Therefore, it is expected that the critical fluctuations of the AFM moments are only weakly coupled to quasiparticles and the superconductivity is mainly induced by the residual interaction between quasiparticles.

3. Spin Fluctuation

First, we investigate the spin fluctuation in the non-centrosymmetric system. To clarify the role of ASOC, we consider the paramagnetic state where $h_Q = 0$. Then, the static spin susceptibility is obtained as

$$\chi^{\mu\nu}(\vec{q}) = \int_0^\beta d\tau \langle T_\tau S^\mu(\vec{q}, \tau) S^\nu(-\vec{q}) \rangle \quad (16)$$

$$= \sum_{s1, s2, s3, s4} \sigma_{s1, s2}^\mu \chi_{1, s1, s2, s3, s4}(\vec{q}) \sigma_{s3, s4}^\nu, \quad (17)$$

where $S^\mu(\vec{q}, \tau) = e^{H\tau} S^\mu(\vec{q}) e^{-H\tau}$ and $S^\mu(\vec{q}) = \sum_{\vec{k}, s, s'} \sigma_{ss'}^\mu c_{\vec{k}+\vec{q}s}^\dagger c_{\vec{k}s}$. We define $\chi_{\max}(\vec{q})$ as the maximum eigenvalue of the 3×3 matrix $\chi^{\mu\nu}(\vec{q})$ for μ and ν .

In the absence of ASOC, the spin susceptibility is isotropic, namely $\chi^{\mu\nu}(\vec{q}) = 0$ for $\mu \neq \nu$ and $\chi^{xx}(\vec{q}) = \chi^{yy}(\vec{q}) = \chi^{zz}(\vec{q}) = \chi_{\max}(\vec{q})$. The spin susceptibility has a peak at $\vec{q} = (0, 0, \pi)$ because of the band structure of the β -band, as shown in Fig. 2(a) (dashed line). Thus,

the β -band favors the ferromagnetic spin correlation in the ab -plane and the AFM correlation between the plane. This is the spin structure realized in the AFM state of CePt₃Si.

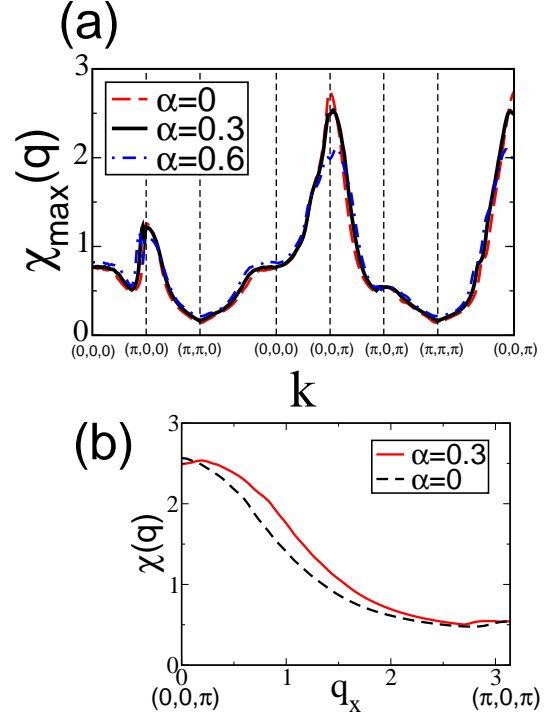


Fig. 2. (color online) (a) Momentum dependence of spin susceptibility $\chi_{\max}(\vec{q})$ in the paramagnetic state ($h_Q = 0$). We assume $U = 4$ and $T = 0.02$ and show the results for $\alpha = 0$ (dashed line), $\alpha = 0.3$ (solid line) and $\alpha = 0.6$ (dash-dotted line). (b) Spin susceptibility $\chi_{\max}(\vec{q})$ along $(0, 0, \pi) - (\pi, 0, \pi)$ direction. We assume $U = 3.95$ for $\alpha = 0$ in (b) so that the maximum spin susceptibilities are similar between $\alpha = 0$ and $\alpha = 0.3$. Numerical calculation is carried out by dividing the first Brillouin zone into a $128 \times 128 \times 48$ lattice.

The anisotropy of spin susceptibility is induced by the ASOC. Our numerical calculation accurately takes into account the ASOC, but we explain here the role of ASOC within the first order of α to provide a simple and qualitative understanding of the helical anisotropy.

The lowest-order term in α appears in the off-diagonal component of the spin susceptibility tensor $\chi^{\mu\nu}(\vec{q})$ which is nonzero unless $\vec{q}_{\parallel} = (n_x, n_y)\pi$ with n_x and n_y integers. The off-diagonal component can be viewed as a result of the Dzyaloshinski-Moriya-type interaction $H_{DM} = \sum_{\vec{q}} iD(\vec{q}) \cdot S(\vec{q}) \times S(-\vec{q})$.⁴¹ Since the Rashba-type ASOC leads to $D(\vec{q}) \propto \alpha \hat{z} \times \vec{q} = \alpha(-q_y, q_x, 0)$ in the vicinity of $\vec{q}_{\parallel} = (0, 0)$, the off-diagonal components of the spin susceptibility tensor are described as $\chi^{yz}(\vec{q}) = -\chi^{zy}(\vec{q}) = i\alpha B(q_z)q_y + O(\alpha^3)$, $\chi^{xz}(\vec{q}) = -\chi^{zx}(\vec{q}) = i\alpha B(q_z)q_x + O(\alpha^3)$, and $\chi^{xy}(\vec{q}) = \chi^{yx}(\vec{q}) = O(\alpha^2)$. Because the momentum dependence of the diagonal component is quadratic as shown by $\chi^{\mu\mu}(\vec{q}_{\parallel}, q_z) \sim \chi(0, q_z) - A(q_z)|\vec{q}_{\parallel}|^2 + O(|\vec{q}_{\parallel}|^4)$, the maximum eigenvalue of the spin susceptibility tensor is obtained as $\chi_{\max}(\vec{q}_{\parallel}, q_z) = \chi(0, q_z) + \alpha B(q_z)|\vec{q}_{\parallel}| - A(q_z)|\vec{q}_{\parallel}|^2 + O(\alpha^2, |\vec{q}_{\parallel}|^4)$ around $\vec{q}_{\parallel} = (0, 0)$. Thus, $\chi_{\max}(\vec{q}_{\parallel}, q_z)$ for each q_z has a local

minimum at $\vec{q}_{\parallel} = 0$ and a local maximum at $\vec{q}_{\parallel} \neq 0$. For $\alpha = 0.3$ the numerical calculation shows four peaks of $\chi_{\max}(\vec{q}_{\parallel}, q_z)$ at $\vec{q} \sim (0, \pm 0.2, \pi)$ and $\vec{q} \sim (\pm 0.2, 0, \pi)$ in contrast to the single peak at $\vec{q} = (0, 0, \pi)$ for $\alpha = 0$ (see Fig. 2(b)).

Since the off-diagonal components, such as $\chi^{xz}(\vec{q}) = (\chi^{zx}(\vec{q}))^*$ and $\chi^{yz}(\vec{q}) = (\chi^{zy}(\vec{q}))^*$, are purely imaginary, the maximum eigenvalue of the spin susceptibility tensor has the eigenvector $\vec{S}(\vec{q}) = \frac{1}{\sqrt{2}}(\tilde{q}_x, \tilde{q}_y, \pm i)$ with $\tilde{q}_{x,y} = q_{x,y}/|\vec{q}_{\parallel}|$. Thus, $\chi_{\max}(\vec{q}_{\parallel}, q_z)$ describes the susceptibility of the helical magnetic order.

We here discuss the effect of higher-order terms of α by which the helical spin structure is distorted. In our result for $\alpha = 0.3$, the spin susceptibility tensor at $\vec{q} = (0.196, 0, \pi)$ has a maximum eigenvalue for $\vec{S}(\vec{q}) \sim (0.81, 0, -0.59i)$. The deviation from $\vec{S}(\vec{q}) = \frac{1}{\sqrt{2}}(1, 0, \pm i)$ in the lowest-order theory of α mainly arises from the second-order term of α in the diagonal component of $\chi^{\mu\nu}(\vec{q})$.

Helical magnetism is suppressed by symmetric spin-orbit coupling, namely, the atomic L - S coupling, which is not taken into account in this paper. This is the reason why the helical magnetic order is not actually realized in non-centrosymmetric heavy fermion compounds, but is observed in non-centrosymmetric compounds with a small L - S coupling.⁷⁵ However, qualitatively the same effects of the ASOC, such as the helical anisotropy of spin susceptibility for $\vec{q}_{\parallel} \neq 0$, are expected in the presence of L - S coupling.

4. Superconductivity

4.1 Pairing symmetry

We examine here the superconductivity. First, we discuss the symmetry of the SC state. It is convenient in the following discussions to describe the order parameter in a standard manner as^{76,77}

$$\Delta_{1,s,s'}(\vec{k}) = \begin{pmatrix} -d_x(\vec{k}) + id_y(\vec{k}) & \Phi(\vec{k}) + d_z(\vec{k}) \\ -\Phi(\vec{k}) + d_z(\vec{k}) & d_x(\vec{k}) + id_y(\vec{k}) \end{pmatrix}, \quad (18)$$

where we use the even parity scalar function $\Phi(\vec{k})$ and the odd parity d -vector $\vec{d}(\vec{k})$. In the presence of the AFM order, the order parameter for the π -triplet and π -singlet pairings $\Delta_{2,s,s'}(\vec{k})$ appears owing to the folding of the Brillouin zone. However, the basic properties and symmetries are hardly affected by π -pairings when $h_Q \ll W$.

We identify two stable solutions of the Éliashberg equation. One pairing state has a predominant p -wave symmetry whose order parameter has the leading odd parity component $\vec{d}(\vec{k}) \sim (-\sin k_y, \beta \sin k_x, 0)$. The parameter β is unity in the absence of the AFM order. The admixed even parity part is approximated as $\Phi(\vec{k}) \sim \delta + \cos k_x + \cos k_y$ with $\delta \sim 0.2$. Thus, the spin singlet component has the s -wave symmetry, as discussed in ref. 24, but its sign changes in the radial direction in order to avoid the local repulsive interaction U . We denote this pairing state as the $s+P$ -wave state.

The other stable solution is the predominantly d -wave state that can be viewed as an interlayer Cooper pairing

state: $\Phi(\vec{k}) \sim \{\sin k_x \sin k_z, \sin k_y \sin k_z\}$ (two-fold degenerate) admixed with an odd-parity component $\vec{d}(\vec{k}) \sim \Phi(\vec{k})(-\sin k_y, \sin k_x, 0)$. In the paramagnetic phase, the most stable combination of the two degenerate states is chiral: $\Phi_{\pm}(\vec{k}) \sim (\sin k_x \pm i \sin k_y) \sin k_z$ which gains the maximal condensation energy in the weak-coupling approach. In the AFM state, however, the two states of $\Phi(\vec{k})$ are no longer degenerate. According to the RPA theory that we adopt in this paper, the d_{xz} -wave state (d_{yz} -wave state) is favored by the AFM order along the \hat{x} -axis (\hat{y} -axis). Since the spin triplet order parameter has both the p -wave and f -wave components, we denote this state as the $p+D+f$ -wave state.

In the RPA theory, superconductivity is assumed to be induced by the spin fluctuation. As discussed in §3, the spin fluctuation arising from the β -band has four peaks around $\vec{q} \sim (0, \pm 0.2, \pi)$ and $\vec{q} \sim (\pm 0.2, 0, \pi)$, which indicates the nearly ferromagnetic (helical) spin correlation in the ab -plane and the AFM coupling between the planes. For a small U , the spin fluctuation has a two-dimensional nature because of the dispersion relation eq. (2). Then, the interplane AFM coupling is negligible and the intraplane nearly ferromagnetic correlation induces $s+P$ -wave superconductivity. On the other hand, the AFM coupling between the planes leads to a three-dimensional spin fluctuation for a large U and favors the $p+D+f$ -wave state. Figure 3 shows the phase diagram against U and the AFM staggered field h_Q . We identify the pairing state with the largest eigenvalue in the Éliashberg equation at $T = 0.02$, as mentioned in §2. We see that the two pairing states are nearly degenerate at around $U = 3 \sim 3.5$ independently of the AFM staggered field.

We find the other pairing state having the predominantly extended s -wave symmetry with $\Phi(\vec{k}) \sim \cos k_x + \cos k_y - 2 \cos k_z$ as a self-consistent solution of the Éliashberg equation. However, we have found no parameter set where this pairing state is stable.

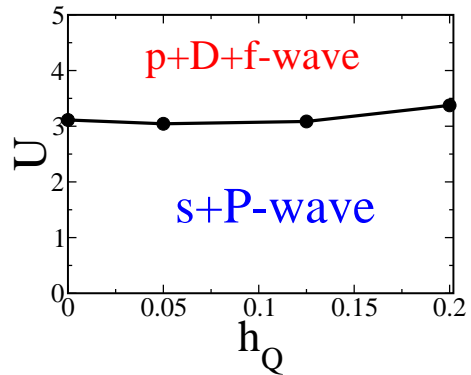


Fig. 3. (color online) Phase diagram against U and h_Q for $\alpha = 0.3$. The $p+D+f$ -wave state ($s+P$ -wave state) is stable for a large (small) U . The solid line shows the boundary of two phases. The Éliashberg equation is solved in the $128 \times 128 \times 32$ lattice.

Next we discuss the stability of the SC state when the ASOC is introduced. Figure 4 shows the α -dependence

of the eigenvalue of the Éliashberg equation λ , for the $s+P$ -wave and $p+D+f$ -wave states. The ASOC has two effects, namely, (i) the spin splitting of the band and (ii) the pairing interaction. The former is quantitatively important in most non-centrosymmetric superconductors where $|\alpha| \geq T_c$. It has been shown that the depairing effect due to (i) is minor for the spin singlet pairing state as well as for the spin triplet one with $\vec{d}(\vec{k}) \parallel \vec{g}(\vec{k})$, while other spin triplet pairing states are destabilized.²⁴ This is the reason why the $s+P$ -wave state having the leading order parameter $\vec{d}(\vec{k}) \sim (-\sin k_y, \beta \sin k_x, 0)$ is favored among p -wave states that have a six-fold degeneracy in the absence of the ASOC and AFM order. Although the depairing effect due to the ASOC is almost avoided in this $s+P$ -wave state, it does not vanish because the relation $\vec{d}(\vec{k}) \parallel \vec{g}(\vec{k})$ is not strictly satisfied in the entire Brillouin zone. It should be noted that the momentum dependence of the vector in the irreducible representation of the point group is not unique. Actually, the momentum dependences of the d -vector $\vec{d}(\vec{k}) \sim (-\sin k_y, \sin k_x, 0)$ and the g -vector $\vec{g}(\vec{k}) = (-v_y(\vec{k}), v_x(\vec{k}), 0)/\bar{v}$ are inequivalent although these vectors are in the same irreducible representation of the C_{4v} point group. Although the momentum dependence of the d -vector is assumed to be the same as that of the g -vector in many theories,^{21, 24–27, 30–32, 53} this assumption is not supported by the microscopic theory since the momentum dependence of the d -vector is mainly determined by the pairing interaction. Thus, Fig. 4 shows a steep decrease in λ in the $s+P$ -wave state when α is turned on. This decrease arises from the depairing effect due to (i), whereby changes in the DOS due to band splitting is an additional source of the α -dependence.

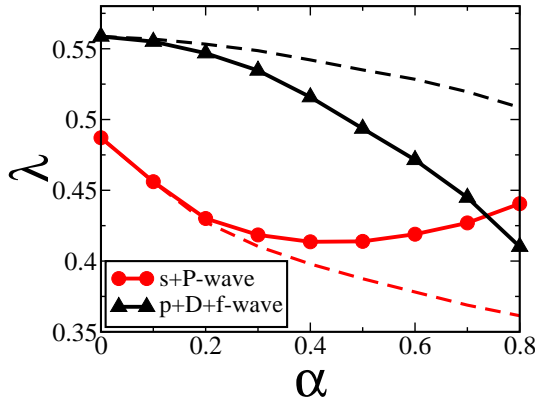


Fig. 4. (color online) Eigenvalues of Éliashberg equation λ for the $s+P$ -wave (circles) and $p+D+f$ -wave states (triangles). We fix $U = 4$ and $h_Q = 0$. The Éliashberg equation is solved in the $128 \times 128 \times 32$ lattice. The dashed lines show λ which is estimated by using the spin susceptibility $\hat{\chi}_i(\vec{q})$ for $\alpha = 0$.

The effect (ii) of ASOC on the pairing interaction originates from the modification of the spin fluctuation. This effect may be important in heavy Fermion systems since a large ASOC is likely induced through a strong L - S coupling in f -orbitals. Figure 2(a) shows the suppression of the spin susceptibility at around $\vec{q} = (0, 0, \pi)$, while

that for other momenta is almost unchanged. Since the spin fluctuations around $\vec{q} = (0, 0, \pi)$ are the main source of the pairing interaction in the $p+D+f$ -wave state, the eigenvalue λ for the $p+D+f$ -wave superconductivity monotonically decreases as $\lambda = \lambda(\alpha = 0) - A\alpha^2/\varepsilon_F^2$. In contrast, the eigenvalue λ for the $s+P$ -wave state shows a minimum and increases with increasing α for $\alpha > 0.4$. Thus, the effect of ASOC on the pairing interaction favors the $s+P$ -wave state rather than the $p+D+f$ -wave state.

These contrasting effects of ASOC arise from the anisotropy of helical spin fluctuation. To clarify this point we show the eigenvalue of Éliashberg equation λ (dashed lines) in which the spin susceptibility $\hat{\chi}_i(\vec{q})$ is estimated for $\alpha = 0$. We see that the λ is increased for the $s+P$ -wave state by the modification of spin susceptibility due to ASOC. Thus, the $s+P$ -wave state is favored by the modified spin fluctuation although the magnitude of spin fluctuation is suppressed at around $\vec{q} = (0, 0, \pi)$ by the ASOC. These results indicate that the anisotropy of helical spin fluctuation enhances the $s+P$ -wave state.

We confirmed that the subdominant component of the order parameter (s -wave component in the $s+P$ -wave state, p - and f -wave components in the $p+D+f$ -wave state) grows almost linearly with increasing α , and that the momentum dependence of each component is almost independent of α .

The eigenvalue of the Éliashberg equation is decreased by the AFM order owing to the loss of quasiparticle DOS. Therefore, the superconductivity is suppressed by the AFM order independently of the pairing symmetry. The relative stability of the $s+P$ -wave and $p+D+f$ -wave states is hardly affected by the AFM order, as shown in Fig. 3. The stability of the interlayer d -wave state against the A-type AFM order has been claimed⁷⁸ by assuming the quasi-two-dimensional Fermi surface. However, this is not the case in our model that assumes the three-dimensional β -band. The T_c of CePt₃Si decreases if the AFM order decreases upon the application of pressure^{58–60} and seems to be incompatible with our result. However, this pressure dependence may be due to the suppression of electron correlation by increasing pressure.

It is expected that the AFM order leads to much more significant depairing effects on the intralayer d -wave and interlayer p -wave states because these Cooper pairings are directly broken by the A-type AFM order. The stability of the SC state against the AFM order^{58–60} implies the interlayer $p+D+f$ -wave or intralayer $s+P$ -wave state in CePt₃Si that is identified in our calculation.

4.2 Superconducting gap

We investigate here the gap structure of both the $s+P$ -wave and $p+D+f$ -wave states and discuss the consistency with the line node behavior observed in CePt₃Si at ambient pressure.^{61–64}

The quasiparticle spectrum in the SC state is obtained by diagonalizing the 8×8 matrix using

$$\hat{H}_s(\vec{k}) = \begin{pmatrix} \hat{H}(\vec{k}) & -\Delta_0 \hat{\Delta}(\vec{k}) \\ -\Delta_0 \hat{\Delta}^\dagger(\vec{k}) & -\hat{H}(-\vec{k})^\top \end{pmatrix}, \quad (19)$$

where $\hat{\Delta}(\vec{k})$ is the SC order parameter in the spin basis expresses as

$$\hat{\Delta}(\vec{k}) = \begin{pmatrix} \Delta_{1,s,s'}(\vec{k}) & \Delta_{2,s,s'}(\vec{k}) \\ \Delta_{2,s,s'}(\vec{k} + \vec{Q}) & \Delta_{1,s,s'}(\vec{k} + \vec{Q}) \end{pmatrix}. \quad (20)$$

In the following calculations the matrix element of $\hat{\Delta}(\vec{k})$ is determined from the linearized Éliashberg equation by assuming that the momentum and spin dependences of the order parameter are weakly dependent on temperature for $T \leq T_c$. We solve the Éliashberg equation at $T = 0.02 > T_c$, having confirmed that the matrix $\hat{\Delta}(\vec{k})$ is almost independent of temperature for $T < 0.1$. The same assumption has been adopted in other studies of multi-orbital superconductivity.^{79,80}

Since the amplitude of the SC order parameter Δ_0 is arbitrary in the linearized Éliashberg equation, we here choose Δ_0 so that the magnitude of the maximal gap is $\Delta_g = 0.1$ in our energy units. Although this magnitude may be large compared with the energy scale α or h_Q , we adopt this value for numerical accuracy, having confirmed that the lower values of Δ_g do not alter the result qualitatively. We define the quasiparticle DOS $\rho(\varepsilon)$ as $\rho(\varepsilon) = \frac{1}{4N} \sum_i \sum_{\vec{k}}' \delta(\varepsilon - E_i(\vec{k}))$ where $\sum_{\vec{k}}'$ denotes the summation within the range $|k_z| < \frac{\pi}{2}$. The eigenvalues $E_8(\vec{k}) > E_7(\vec{k}) > \dots > E_1(\vec{k})$ satisfy the relation $E_i(\vec{k}) = -E_{9-i}(\vec{k})$.

It is more transparent to describe the SC order parameter in the band basis, which is obtained by unitary transformation using

$$\hat{\Delta}_{\text{band}}(\vec{k}) = \hat{U}^\dagger(\vec{k}) \hat{\Delta}(\vec{k}) \hat{U}^*(-\vec{k}). \quad (21)$$

The unitary matrix $\hat{U}(\vec{k})$ diagonalizes the unperturbed Hamiltonian as

$$\hat{U}^\dagger(\vec{k}) \hat{H}(\vec{k}) \hat{U}(\vec{k}) = (e_i(\vec{k}) \delta_{ij}). \quad (22)$$

The SC gap in the γ -th band is obtained as

$$\Delta_\gamma(\vec{k}) = \Delta_0 \Psi_\gamma(\vec{k}), \quad (23)$$

where $\Psi_\gamma(\vec{k})$ is the $(\gamma\gamma)$ component of the matrix $\hat{\Delta}_{\text{band}}(\vec{k})$. Since the relation $T_c \ll |\alpha|$ is satisfied in most of the non-centrosymmetric superconductors, the relation $|\Delta_{\text{band}}^{ij}(\vec{k})| \ll |\alpha \hat{g}(\vec{k})|, \max\{h_Q, |\varepsilon(\vec{k}) - \varepsilon(\vec{k} + \vec{Q})|\}$ is valid for each (ij) component of $\hat{\Delta}_{\text{band}}(\vec{k})$ except for the special momentum such as $\vec{k} = (0, 0, k_z)$. Therefore, the off-diagonal components of $\hat{\Delta}_{\text{band}}(\vec{k})$ hardly affect the electronic state, and the quasiparticle excitations $E_i(\vec{k})$ are approximated to $\pm E_\gamma^{\text{band}}(\vec{k})$ with $E_\gamma^{\text{band}}(\vec{k})^2 = e_\gamma(\vec{k})^2 + |\Delta_\gamma(\vec{k})|^2$. Thus, the SC gap in the γ -th band is described by $|\Delta_\gamma(\vec{k})|$.

It is clear that the $p+D+f$ -wave state has a horizontal line node protected by the symmetry because all of the matrix elements of $\hat{\Delta}(\vec{k})$ are zero at $k_z = 0$. This is consistent with the experiments in CePt₃Si.^{61–64} The coefficient c_1 of the linear term in the DOS ($\rho(\varepsilon) = c_1 \varepsilon$) increases in the AFM state because the pairing state changes from the chiral $d_{xz} \pm i d_{yz}$ -wave state in the paramagnetic state to the d_{xz} -wave state in the AFM state (see Fig. 3 of ref. 28).

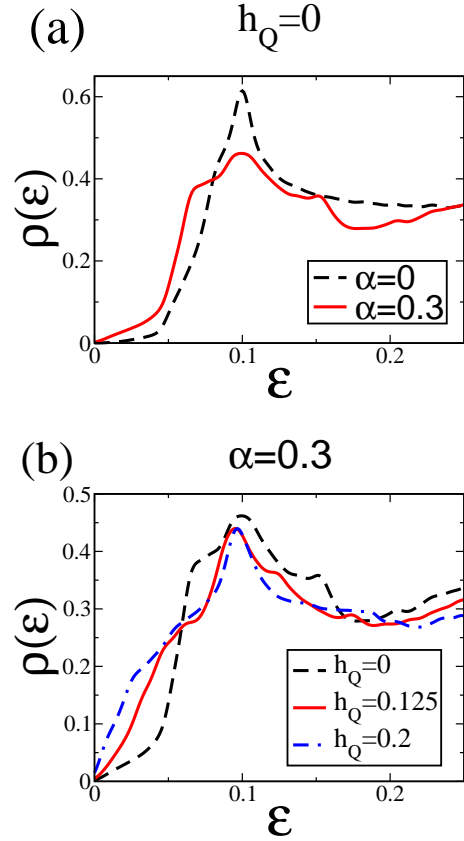


Fig. 5. (color online) DOS $\rho(\varepsilon)$ in the $s+P$ -wave state at $U = 4$. (a) Paramagnetic state for $\alpha = 0$ (dashed line) and 0.3 (solid line). (b) AFM state with ASOC $\alpha = 0.3$ for $h_Q = 0.125$ (solid line) and $h_Q = 0.2$ (dash-dotted line). We show the results for $\varepsilon > 0$ because $\rho(\varepsilon)$ is particle-hole symmetric owing to its definition. The Éliashberg equation is solved in the $64 \times 64 \times 32$ lattice and the DOS is calculated in the $384 \times 384 \times 384$ lattice.

We investigate here the accidental line node of the SC gap in the $s+P$ -wave state in detail. The quasiparticle DOS $\rho(\varepsilon)$ is shown in Fig. 5 and the SC gaps $|\Delta_\gamma(\vec{k})|$ for $\gamma = 3, 4$ are shown in Figs. 6 and 7, respectively. The paramagnetic state is assumed in Fig. 6, while the AFM state is assumed in Fig. 7.

The SC gap in the absence of the ASOC and AFM order (Fig. 6(a)) is approximated to be $|\Delta(\vec{k})| \sim \sqrt{\sin^2 k_x^2 + \sin^2 k_y^2}$, which has two point nodes in the $[001]$ direction in contrast to the experimental results.^{61–64} The DOS at low energies is quadratic as shown by $\rho(\varepsilon) \sim c_2 \varepsilon^2$ and the coefficient c_2 is small owing to the small DOS in the $[001]$ direction (dashed line in Fig. 5(a)).

The line nodes are induced by the ASOC through the following two mechanisms.

- (I) Admixture with an s -wave order parameter.
- (II) Mismatch of the d -vector and g -vector.

The first one (I) has been proposed by Frigeri *et al.*⁴¹ and its contributions to the NMR $1/T_1 T$ and superfluid density have been investigated by Hayashi *et al.*^{30,32} In the absence of the AFM order, the SC gap is expressed as $\pm \Phi(\vec{k}) + \vec{d}(\vec{k}) \cdot \vec{g}(\vec{k})$ with $\vec{g}(\vec{k}) = \vec{g}(\vec{k})/|\vec{g}(\vec{k})|$. The s -wave and p -wave order parameters are approximated to be $\Phi(\vec{k}) \sim \Phi(\vec{0}, k_z)$ and $\vec{d}(\vec{k}) \cdot \vec{g}(\vec{k}) \sim c(k_z)|\vec{k}_\parallel|$ at around

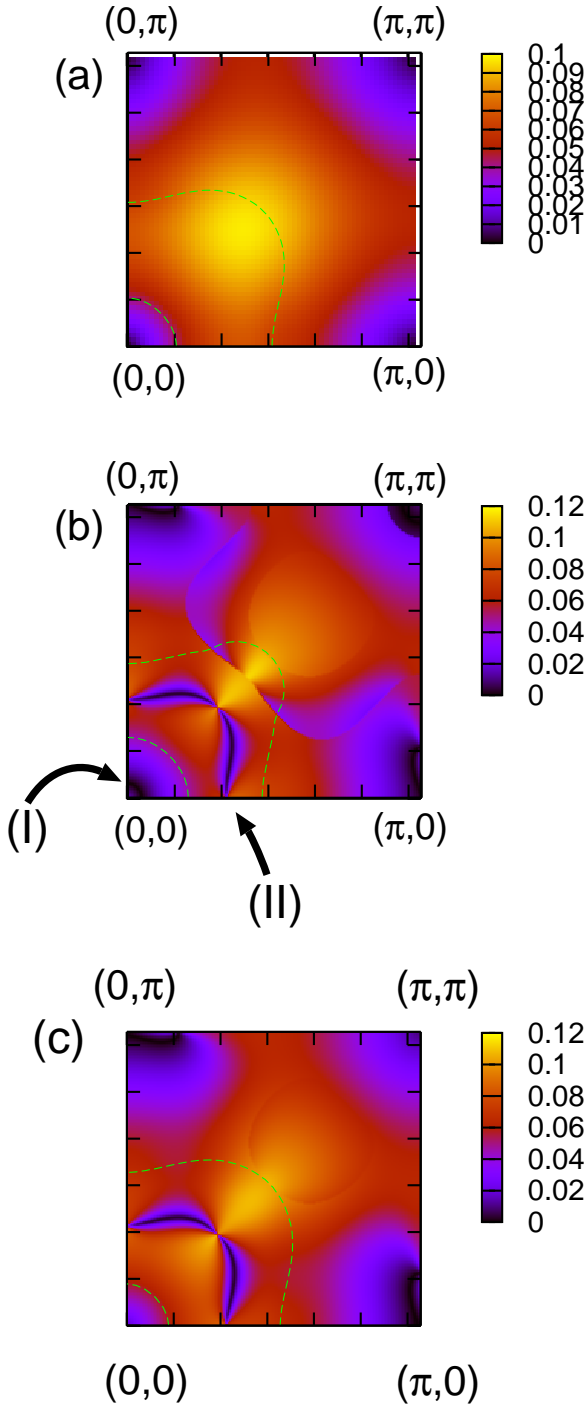


Fig. 6. (color online) SC gap in the $s+P$ -wave state at $k_z = \frac{\pi}{3}$ in the paramagnetic state ($h_Q = 0$). (a) SC gap in the absence of the ASOC ($\alpha = 0$). We show the SC gaps $|\Delta_3(\vec{k})|$ and $|\Delta_4(\vec{k})|$ for $\alpha = 0.3$ in (b) and (c), respectively. The SC gaps $|\Delta_1(\vec{k})|$ and $|\Delta_2(\vec{k})|$ are not shown because the quasiparticle DOS is small in these bands. The positions of the line nodes arising from the mechanisms (I) and (II) are shown by the arrows in (b) (see the text). The thin dashed lines show the Fermi surface at $k_z = \frac{\pi}{3}$. Although the zeros of SC gap do not intersect with the Fermi surface at $k_z = \frac{\pi}{3}$, the line nodes exist on the Fermi surface at another k_z . Note that the β -band has a three-dimensional Fermi surface, while the SC gap in the $s+P$ -wave state is nearly independent of k_z .

$\vec{k}_{\parallel} = (k_x, k_y) = (0, 0)$, respectively. Therefore, the SC gap vanishes on the line $|\vec{k}_{\parallel}| = |\Phi(\vec{0}, k_z)|/c(k_z)$ in half of the bands, while the other bands have a full gap. We show the SC gaps $|\Delta_3(\vec{k})|$ and $|\Delta_4(\vec{k})|$ at $k_z = \pi/3$ in Figs. 6(b) and 6(c), respectively. The line node actually appears in $|\Delta_3(\vec{k})|$ in the vicinity of $\vec{k}_{\parallel} = (0, 0)$ (shown by the arrow (I)). However, the line node arising from the mechanism (I) induces only a tiny linear term $\rho(\varepsilon) \sim c_1 \varepsilon$ with $c_1 \propto |\alpha|$ because the length of the line node is very small, as shown in Fig. 6(b).

We find another line node arising from the mechanism (II) at around $|k_{\parallel}| = \pi/3$ (see the arrow (II) in Fig. 6(b)). This line node originates from the topological character of the g -vector. According to the assumptions $g_x(\vec{k}) = -v_y(\vec{k})/\bar{v}$ and $g_y(\vec{k}) = v_x(\vec{k})/\bar{v}$, the g -vector has a singularity not only on the $[001]$ line but also on the line at around $(k_x, k_y) = (0.4\pi, 0.4\pi)$. The g -vector rotates around the singular point, and therefore the relation $\vec{d}(\vec{k}) \perp \vec{g}(\vec{k})$ is satisfied on a line. The SC gap $\pm \Phi(\vec{k}) + \vec{d}(\vec{k}) \cdot \vec{g}(\vec{k})$ vanishes around this line because the s -wave component $|\Phi(\vec{k})|$ is much smaller than the p -wave component $|\vec{d}(\vec{k})|$. This is a general mechanism for the line node in the non-centrosymmetric superconductor predominated by the spin triplet pairing. However, it is not clear whether this line node exists in CePt₃Si because it depends on the detailed momentum dependence of the g -vector. For example, this line node does not appear if we assume $\vec{g}(\vec{k}) = (-\sin k_y, \sin k_x, 0)$. Anyway, the low-energy excitation arising from the ASOC is small because of the steep increase in SC gap around the line node, as shown in the schematic figure (Fig. 8). Figure 5(a) actually shows a small coefficient c_1 of the linear term $\rho(\varepsilon) = c_1 \varepsilon$ (solid line). This linear term mainly arises from the line node induced by the mechanism (II) and the contribution of the line node (I) is negligible.

The DOS at low energies is markedly increased by the AFM order owing to the following two effects.

(III) Folding of the Brillouin zone.

(IV) Mixing of the p -wave order parameter between the leading part $\vec{d}(\vec{k}) \sim (-\sin k_y, \sin k_x, 0)$ and the admixed part $\hat{d}(\vec{k}) = (\sin k_y, \sin k_x, 0)$.

The former arises from the pair-breaking effect due to the band mixing, which has been investigated by Fujimoto.³¹ In contrast to ref. 31, the line node appears not only at $k_z = \pi/2$ but also at around $(k_x, k_y) = (\pi/2, \pi/2)$ (see Fig. 7(b)) in our case because of the band structure of the β -band. However, the DOS arising from (III) is not quantitatively important when $h_Q \ll W$ because of the steep increase in the SC gap around the line node, as shown in Fig. 8.

Actually, the low-energy excitations in the $s+P$ -wave state are mainly induced by the effect (IV). The a - and b -axes in the tetragonal lattice are no longer equivalent in the presence of the AFM order. Therefore, the p -wave order parameter is modified to $\vec{d}(\vec{k}) = (-\sin k_y, \beta \sin k_x, 0)$ with $\beta \neq 1$. This change can be viewed as the mixing of the leading part $\vec{d}(\vec{k}) = (-\sin k_y, \sin k_x, 0)$ with the admixed part $\hat{d}(\vec{k}) = (\sin k_y, \sin k_x, 0)$, which leads to the rotation of the d -vector. According to the result ob-

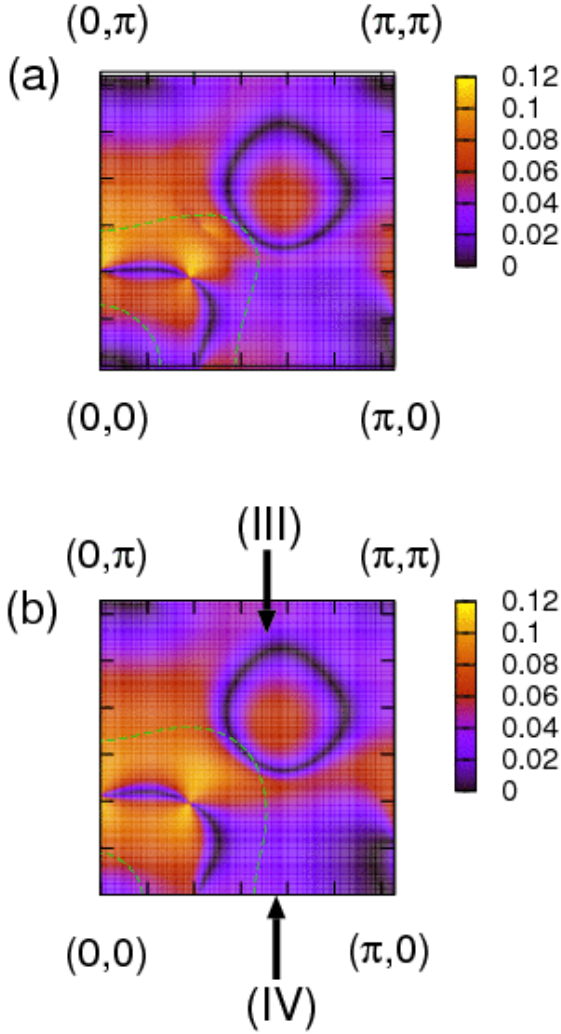


Fig. 7. (color online) SC gap in the $s+P$ -wave state with the AFM order. We show (a) $|\Delta_3(\vec{k})|$ and (b) $|\Delta_4(\vec{k})|$ at $k_z = \frac{\pi}{3}$ for $\alpha = 0.3$ and $h_Q = 0.125$. The positions of the line nodes arising from the mechanism (III) and (IV) are shown by the arrows in (b).

tained using the RPA theory, β decreases with increasing h_Q . Then, many low-energy excitations are induced at around $k_y = \pi/6$, as shown in Fig. 7(b). The SC gap in the 4-th band (Fig. 7(b)) is further decreased at around $k_y = \pi/6$ by the admixture with an s -wave order parameter. The DOS clearly shows a linear dependence in Fig. 5(b), which is consistent with the experimental results in CePt₃Si at ambient pressure.^{61–64} We have shown that the rotation of the d -vector is also the main source of the anomalous paramagnetic properties of CePt₃Si.²⁹

4.3 Specific heat and NMR $1/T_1T$

The pressure dependence of the SC state is a decisive test for validating the theory of CePt₃Si as well as of CeRhSi₃ and CeIrSi₃. According to the experimental result of CePt₃Si,^{58–60} the AFM order is suppressed at a pressure $P \sim 0.6$ GPa, although the superconductivity survives at high pressures $P > 0.6$ GPa. Therefore, the role of the AFM order can be studied experimentally by measuring the pressure dependence of the SC state.

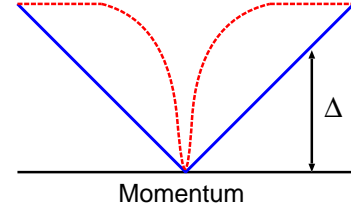


Fig. 8. (color online) Schematic figure showing the momentum dependence of SC gap along the Fermi surface. The solid line shows the usual line node protected by the symmetry (for example, the $d_{x^2-y^2}$ -wave superconductor). The accidental line nodes (II) in Fig. 6(b) and (III) in Fig. 7(b) show a steep increase in the SC gap around the gap node (dashed line).

If the $s+P$ -wave state is realized in CePt₃Si and the AFM order is the main source of line nodes, the number of low-energy excitations decreases under pressure. This theoretical result can be tested by measuring the pressure dependence of specific heat, NMR $1/T_1T$, superfluid density, thermal conductivity, and other quantities. We now calculate specific heat and NMR $1/T_1T$ for a future experimental test.

To discuss these quantities, we adopt the same assumption in §4.2. We here calculate the amplitude of the SC gap, Δ_0 , in eq. (19) by solving the gap equation

$$1 = g \sum_k |\Psi_\gamma(\vec{k})|^2 \tanh \frac{E_\gamma^{\text{band}}(\vec{k})}{2T} / 2E_\gamma^{\text{band}}(\vec{k}), \quad (24)$$

which is obtained as a mean field solution of the effective model in the band basis given as

$$H = \sum_k \sum_{\gamma=1}^4 e_\gamma(\vec{k}) d_{\vec{k},\gamma}^\dagger d_{\vec{k},\gamma} - \frac{1}{2} g \sum_{k,k'} b_k^\dagger b_{k'}, \quad (25)$$

$$b_k^\dagger = \sum_\gamma \Psi_\gamma(\vec{k}) d_{\vec{k},\gamma}^\dagger d_{-\vec{k},\gamma}^\dagger. \quad (26)$$

The SC order parameter obtained in the linearized Éliashberg equation (eqs. (5)-(7)) is reproduced using this model. We choose g so as to obtain $T_c = 0.05$. We have confirmed that the smaller g and T_c do not qualitatively alter the following results.

The quasiparticle excitation $E_i(\vec{k})$ is determined using eq. (19) with Δ_0 determined using eq. (24). The Sommerfeld coefficient C/T is obtained as

$$C/T = \frac{\partial S}{\partial T}, \quad (27)$$

$$S = - \sum_k \sum_{i=1}^8 [f_{i,\vec{k}} \log f_{i,\vec{k}} + (1 - f_{i,\vec{k}}) \log(1 - f_{i,\vec{k}})], \quad (28)$$

where $f_{i,\vec{k}}$ is the Fermi distribution function $f_{i,\vec{k}} = (1 + \exp(E_i(\vec{k})/T))^{-1}$.

We calculate NMR $1/T_1T$ as

$$1/T_1T = \text{Im} \chi_L(\Omega) / \Omega|_{\Omega \rightarrow 0}, \quad (29)$$

$$\chi_L(i\Omega_n) = - \sum_{\vec{k}, \vec{k}', \omega_n} \sum_{i=1}^2 [G_{i,\uparrow}(\vec{k}', i\omega_n + i\Omega_n) G_{i,\downarrow}(\vec{k}, i\omega_n) - F_{i,\downarrow}^\dagger(\vec{k}', i\omega_n + i\Omega_n) F_{i,\uparrow}(\vec{k}, i\omega_n)], \quad (30)$$

where $\hat{G}_i(\vec{k}, i\omega_n)$ and $\hat{F}_i(\vec{k}, i\omega_n)$ are the normal and anomalous Green functions in the SC state, respectively. We ignore the momentum dependence of the hyperfine coupling constant and the exchange enhancement due to the electron correlation for simplicity. The local spin susceptibility $\chi_L(\Omega)$ is obtained from $\chi_L(i\Omega_n)$ through the analytic continuation.

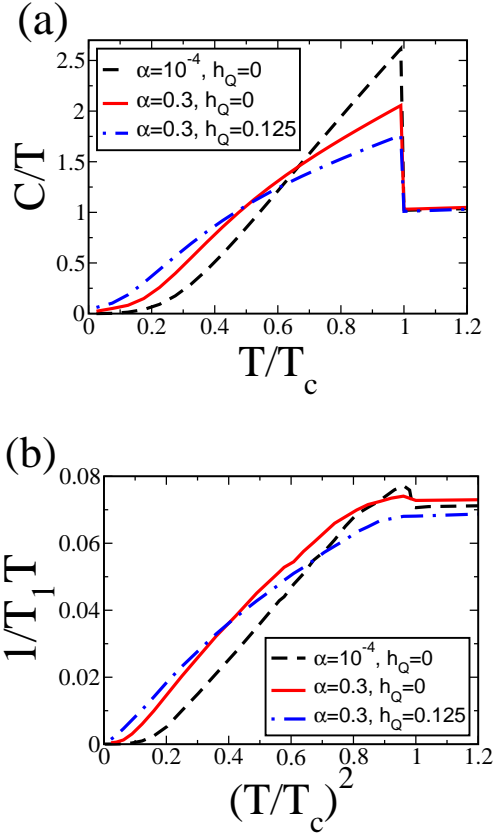


Fig. 9. (color online) (a) Sommerfeld coefficient C/T and (b) NMR $1/T_1T$ in the $s+P$ -wave state. The parameters α and h_Q are shown in the figure. We solve the Éliashberg equation in $64 \times 64 \times 32$ lattices and estimate C/T and $1/T_1T$ in $384 \times 384 \times 192$ lattices.

Figures 9(a) and 9(b) respectively show the temperature dependences of the Sommerfeld coefficient C/T and the NMR $1/T_1T$ in the $s+P$ -wave state. When we assume a weak ASOC ($|\alpha| \ll T_c$) and the absence of the AFM order (dashed lines in Fig. 9), both the Sommerfeld coefficient and the NMR $1/T_1T$ at low temperatures are much smaller than those expected in the superconductor with line nodes. For example, the Sommerfeld coefficient shows a T^n dependence ($n > 2$) which is incompatible with the experimental result.⁶³ On the other hand, we clearly see the line node behavior in the presence of the ASOC and AFM order (dash-dotted lines in Fig. 9). The Sommerfeld coefficient obeys the T -linear law and the

NMR $1/T_1T$ shows a T^2 dependence at low temperatures. These results are consistent with the experimental data of specific heat,⁶³ thermal conductivity,⁶¹ superfluid density,⁶² and NMR $1/T_1T$.⁶⁴

Upon decreasing the staggered field h_Q , low-energy excitations are suppressed. In the paramagnetic state ($h_Q = 0$), the Sommerfeld coefficient deviates from the T -linear law below $T < 0.2T_c$, while the T^2 dependence of NMR $1/T_1T$ breaks down at lower temperatures, $T < 0.1T_c$ (solid lines in Fig. 9). If the AFM order is the main source of the line node in CePt₃Si at ambient pressure, these deviations from the line node behavior may be observed at high pressures $P > 0.6\text{GPa}$.

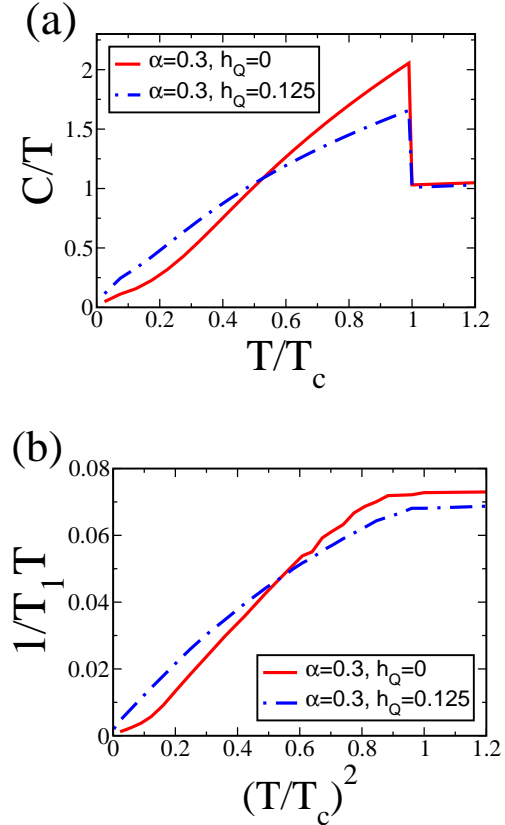


Fig. 10. (color online) (a) Sommerfeld coefficient C/T and (b) NMR $1/T_1T$ in the $p+D+f$ -wave state.

Figure 10 shows the Sommerfeld coefficient and NMR $1/T_1T$ in the $p+D+f$ -wave state. The line node behavior appears clearly in both the paramagnetic and AFM states. The role of the AFM order is qualitatively the same as that in the $s+P$ -wave state: the number of low-energy excitations is increased by the AFM order. This is because the vertical line node in the d_{xz} -wave state disappears in the chiral d -wave state.

We here discuss the coherence peak in the NMR $1/T_1T$. It has been shown that the coherence peak appears in the $s+P$ -wave state just below T_c owing to the finite coherence factor.^{20,30} This is the case in our calculation; however, the coherence peak is much smaller than that shown in ref. 30, as shown in Fig. 9(b). This is because of the small ASOC $\alpha = 0.3 \ll \varepsilon_F$ assumed in

this paper and the extended s -wave nature of the spin singlet order parameter. The coherence factor in the extended s -wave state is decreased by the sign reversal of the order parameter in the radial direction. Note that the isotropic s -wave pairing is generally not favored in the strongly correlated electron systems. A slightly larger coherence peak appears in the paramagnetic state (solid line in Fig. 9(b)); however, this is not due to the coherence factor but arises from the anomaly in the DOS. Although a coherence peak was reported in the early measurement of NMR $1/T_1T$,⁵⁶ the recent measurement for a clean sample shows no coherence peak just below T_c ,⁶⁴ in agreement with our result.

4.4 Multiple phase transitions

We have discussed the pressure dependence of low-energy excitations in §4.2 and §4.3. Although qualitatively the same results are obtained for the low-energy excitations between the $s+P$ -wave and $p+D+f$ -wave states, there is an essential difference, namely, the multiple phase transitions in the P - T plane. To illustrate this issue, we show the possible phase diagrams in Fig. 11.

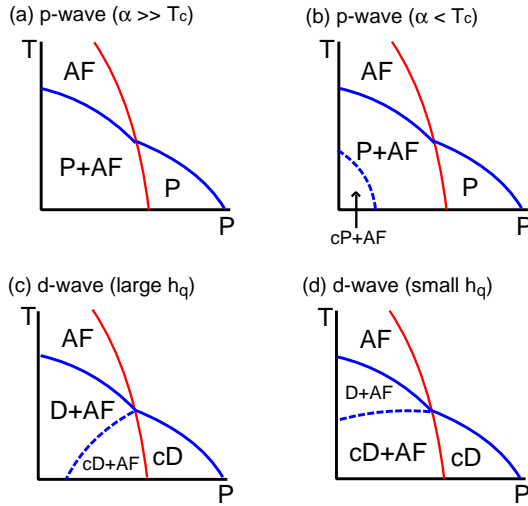


Fig. 11. (color online) Possible phase diagrams in the P - T plane. (a) $s+P$ -wave state for a large ASOC ($|\alpha| \gg T_c$). (b) $s+P$ -wave state for a small ASOC ($|\alpha| \leq T_c$). (c) $p+D+f$ -wave state for a large staggered field h_Q . (d) $p+D+f$ -wave state for a small staggered field. “D” (“cD”) shows the d_{xz} -wave (chiral $d_{xz} \pm id_{yz}$ -wave) state. “cP” shows the chiral p -wave state where the dominant order parameter is $\vec{d} = (p_x \pm ip_y)\hat{x}$.

Figures 11(a) and 11(b) show the phase diagrams in the $s+P$ -wave state. When the ASOC is small ($|\alpha| \leq T_c$), the chiral p -wave state is stabilized at low temperatures and low pressures, as in Fig. 11(b). However, this is unlikely for CePt₃Si since the ASOC is much larger than T_c in heavy fermion systems. Therefore, the simple phase diagram in Fig. 11(a) is expected in the $s+P$ -wave state of CePt₃Si.

In the case of the $p+D+f$ -wave state, the phase transition from the chiral $d_{xz} \pm id_{yz}$ -wave state to the d_{xz} -wave state must occur, as in Fig. 11(c) or 11(d). When the staggered field h_Q is large (small) at ambient pressure,

the phase diagram in Fig. 11(c) (Fig. 11(d)) is expected. Thus, the enhancement of the low-energy DOS due to pressure accompanies the second order phase transition, in contrast to the $s+P$ -wave state. The observation of a multiple phase transition in the P - T plane might provide clear evidence of the $p+D+f$ -wave case. Although the second SC transition has been observed in CePt₃Si,^{62,81} it has been shown that there are two SC phases with $T_c \sim 0.75\text{K}$ and $T_c \sim 0.45\text{K}$ in the sample.^{63,81–83} The second transition below T_c seems to be caused by sample inhomogeneity.

4.5 Anisotropy of upper critical field H_{c2}

We here comment on the in-plane anisotropy of H_{c2} arising from the AFM order. As discussed in §4.2, the p -wave order parameter in the $s+P$ -wave $\vec{d}(\vec{k}) \sim (-\sin k_y, \beta \sin k_x, 0)$ has a two-fold in-plane anisotropy in the AFM state. The anisotropy parameter β can be measured by the in-plane anisotropy of H_{c2} near T_c , which is determined by the orbital depairing effect and written as $H_{c2}^a = \Phi_0/(2\pi\xi_b\xi_c)$ and $H_{c2}^b = \Phi_0/(2\pi\xi_a\xi_c)$ for $\vec{H} \parallel \hat{a}$ and $\vec{H} \parallel \hat{b}$, respectively. Here, $\Phi_0 = \frac{hc}{2e}$ is the flux quantum and $\xi_{a,b,c} = \xi_{a,b,c}^0(1 - T/T_c)^{-1/2}$ are coherence lengths. We obtain the ratio of the gradient $H_{c2}^{a,b,c} = -T_c dH_{c2}^{a,b,c}/dT$ as, $H_{c2}^a : H_{c2}^b : H_{c2}^c = \xi_a^0 : \xi_b^0 : \xi_c^0$ which can be estimated using the relation, $(\xi_{a,b,c}^0)^2 \propto \sum_{\gamma,k} v_{\gamma,a,b,c}^2(\vec{k}) |\Psi_{\gamma}(\vec{k})|^2 f''(e_{\gamma}(\vec{k}))/8e_{\gamma}(\vec{k})$, where $v_{\gamma,a,b,c}(\vec{k}) = de_{\gamma}(\vec{k})/dk_{a,b,c}$ is the quasiparticle velocity in the γ -th band.

Figure 12 shows the in-plane anisotropy H_{c2}^a/H_{c2}^b in the $s+P$ -wave state (solid line). It is clearly shown that the anisotropy is induced by the AFM order for $h_Q > 0.1$. This is mainly due to the decrease in the anisotropy parameter β . Since $\beta < 1$ in the RPA theory and we assume the AFM staggered moment pointing along the a -axis, H_{c2} is higher along the b -axis than along the a -axis ($H_{c2}^a < H_{c2}^b$). If $\beta > 1$, the opposite anisotropy appears. Thus, if the marked mixing of p -wave order parameters due to the AFM order occurs, a pronounced in-plane anisotropy appears in H_{c2} .

The paramagnetic depairing effect qualitatively induces the same in-plane anisotropy as that in Fig. 12. We have shown in ref. 29 a schematic figure of the H - T phase diagram by taking into account both the orbital and paramagnetic depairing effects.

The in-plane anisotropy of H_{c2} in the $p+D+f$ -wave state is quite different from that in the $s+P$ -wave state. We obtain $H_{c2}^a/H_{c2}^b \sim 1.6$ in the $p+D+f$ -wave state independent of the nonzero staggered field h_Q . This two-fold anisotropy changes discontinuously way from $H_{c2}^a/H_{c2}^b \sim 1.6$ in the AFM state to $H_{c2}^a/H_{c2}^b = 1$ in the paramagnetic state, in contrast to the continuous change in the $s+P$ -wave state. It is therefore expected that the $s+P$ -wave state can be distinguished from the $p+D+f$ -wave state by the pressure dependence of in-plane anisotropy in H_{c2} .

Next we comment on the experimental measurement of in-plane anisotropy arising from the AFM order. The direction of the AFM moment can be controlled by the cooling process, namely zero-field cooling and field cool-

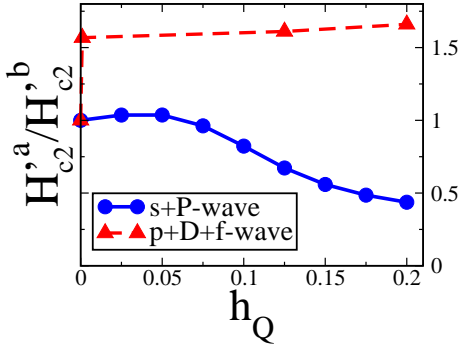


Fig. 12. (color online) In-plane anisotropy of H_{c2} in the $s+P$ -wave (solid line) and $p+D+f$ -wave (dashed line) states. We assume $\alpha = 0.3$. We show the ratio of the gradient $H'_{c2}^a = -T_c dH_{c2}^a/dT$ and $H'_{c2}^b = -T_c dH_{c2}^b/dT$ where H_{c2}^a and H_{c2}^b are the upper critical fields along a - and b -axes, respectively.

ing. When temperature is decreased under the magnetic field along the b -axis, the AFM moment parallel to the a -axis appears below the Néel temperature, because the system gains the maximum magnetic energy when the AFM moment is perpendicular to the magnetic field. Then, the two-fold anisotropy due to the AFM order appears at low magnetic fields, although the AFM moment may rotate at high magnetic fields. On the other hand, the domain structure with respect to the direction of AFM moment can appear when the system is cooled under a zero magnetic field. Then the two-fold anisotropy is obscured.

Before closing this section, some comments are given on the anisotropy of H_{c2} between the ab -plane and the c -axis. We cannot discuss this anisotropy in a final way because not only the β -band but also the other band affects the anisotropy. However, it should be noted that H_{c2} is of similar magnitude along the ab -plane and the c -axis because the β -band has a three-dimensional Fermi surface. For example, we obtain $H'_{c2}^a : H'_{c2}^b : H'_{c2}^c = 1 : 1 : 0.71$ for $h_Q = 0$ and $H'_{c2}^a : H'_{c2}^b : H'_{c2}^c = 0.67 : 1 : 0.55$ for $h_Q = 0.125$ in the $s+P$ -wave state, while $H'_{c2}^a : H'_{c2}^b : H'_{c2}^c = 1 : 1 : 0.85$ for $h_Q = 0$ and $H'_{c2}^a : H'_{c2}^b : H'_{c2}^c = 1.61 : 1 : 0.86$ for $h_Q = 0.125$ in the $p+D+f$ -wave state. The weak anisotropy of H_{c2} between $H \parallel ab$ and $H \parallel c$ is consistent with the experimental result for CePt₃Si.⁵⁸

5. Summary and Discussion

We have investigated the superconductivity in the Hubbard model with Rashba-type spin-orbit coupling and AFM order. Applying the RPA theory to the β -band of CePt₃Si, we found two stable pairing states, the intraplane p -wave state admixed with the s -wave component ($s+P$ -wave state) and the interplane d -wave state admixed with the p - and f -wave components ($p+D+f$ -wave state). We found that the anisotropy of helical spin fluctuation favors the $s+P$ -wave state.

We examined the low-energy excitations in detail. The SC gap in the $p+D+f$ -wave state has a line node protected by the symmetry, while accidental line nodes appear in the $s+P$ -wave state. Thus, both pairing states seem to be consistent with the experimental results in

CePt₃Si at ambient pressure.^{61–64} A substantial part of the accidental line node in the $s+P$ -wave state can be induced by the AFM order through the rotation of the d -vector. The line node in the $p+D+f$ -wave state is also increased by the AFM order because of the phase transition from the chiral d -wave state in the paramagnetic state to the d_{xz} -wave state in the AFM state. Thus, the number of low-energy excitations decreases in both states when the AFM order is suppressed by pressure. We calculated the specific heat and NMR $1/T_1T$ in both the paramagnetic and AFM states. The deviation from the line node behavior in the paramagnetic state has been pointed out.

We proposed some future experiments that can elucidate the pairing state in CePt₃Si. The first one is the pressure dependence of low-energy excitations discussed above. Another one is the possible multiple SC phase transitions in the P - T -plane. The second SC transition occurs below T_c near the critical pressure for the AFM order, if the $p+D+f$ -wave superconductivity is realized. This is in contrast to the $s+P$ -wave state where no additional phase transition is expected. The marked change of low-energy excitations in the $p+D+f$ -wave state is accompanied by the second order phase transition. The last proposal is the anisotropy of H_{c2} in the ab -plane. In the $s+P$ -wave state, the anisotropy of H_{c2} gradually increases with increasing AFM moment, while that in the $p+D+f$ -wave state is discontinuous at a critical pressure for the AFM order. Our proposals for future experiments do not rely on the particular band structure of the β -band in CePt₃Si, and therefore can also be applied to CeRhSi₃, CeIrSi₃, and CeCoGe₃.

According to the present experiments, the $s+P$ -wave superconductivity is most likely realized in CePt₃Si. The paramagnetic properties measured on the basis of the NMR Knight shift and H_{c2} seem to be compatible with those in the $s+P$ -wave state.²⁹ Further studies from both the theoretical and experimental points of view are highly desired to elucidate the novel physics in the non-centrosymmetric superconductivity.

Acknowledgments

The authors are grateful to D. F. Agterberg, J. Akimitsu, S. Fujimoto, J. Flouquet, N. Hayashi, R. Ikeda, K. Izawa, N. Kimura, Y. Kitaoka, Y. Matsuda, M.-A. Measson, V. P. Mineev, G. Motoyama, H. Mukuda, Y. Onuki, T. Shibauchi, R. Settai, T. Tateiwa, and M. Yogi for fruitful discussions. This study was financially supported by the Nishina Memorial Foundation, Grants-in-Aid for Young Scientists (B) from MEXT, Japan, Grants-in-Aid for Scientific Research on Priority Areas (No. 17071002) from MEXT, Japan, the Swiss Nationalfonds, and the NCCR MaNEP. Numerical computation in this work was carried out at the Yukawa Institute Computer Facility.

Appendix: Derivation of Rashba-type ASOC in Tight-binding Models

We here microscopically derive the Rashba-type spin-orbit coupling in the periodical Anderson model and Hubbard model by tight-binding approximation.

The localized $4f$ states in the Ce-based heavy fermion

superconductors, such as CePt₃Si, CeRhSi₃, and CeIrSi₃ are described by the $J = 5/2$ manifold whose degeneracy is split by the crystal electric field. The $4f$ levels in CePt₃Si are described by the three doublets,⁸⁴

$$|\Gamma_{7\pm}\rangle = \sqrt{\frac{5}{6}}|\pm \frac{5}{2}\rangle - \sqrt{\frac{1}{6}}|\mp \frac{3}{2}\rangle, \quad (\text{A}\cdot 1)$$

$$|\Gamma'_{6\pm}\rangle = |\pm \frac{1}{2}\rangle, \quad (\text{A}\cdot 2)$$

$$|\Gamma'_{7\pm}\rangle = \sqrt{\frac{1}{6}}|\pm \frac{5}{2}\rangle + \sqrt{\frac{5}{6}}|\mp \frac{3}{2}\rangle. \quad (\text{A}\cdot 3)$$

The ground state is $|\Gamma_{7\pm}\rangle$, and the excited $|\Gamma'_{6\pm}\rangle$ and $|\Gamma'_{7\pm}\rangle$ states have excitation energies of 1 and 24 meV, respectively.⁵⁷

Next we construct a periodical Anderson model for the $|\Gamma_{7\pm}\rangle$ state, which hybridizes with conduction electrons. It is straightforward to apply the following procedure to the $|\Gamma'_{6\pm}\rangle$ and $|\Gamma'_{7\pm}\rangle$ states. Because the mirror symmetry is broken along the z -axis in CePt₃Si, the odd parity Ce $4f$ -orbital is hybridized with the even parity s - and d -orbitals in the same Ce site. Owing to the symmetry of the $|\Gamma_{7\pm}\rangle$ state, the localized $4f$ state is hybridized with the d_{xy} -, d_{xz} - and d_{yz} -orbitals. Then, the wave function of the localized state can be expressed as,

$$|f\pm\rangle = \kappa|\Gamma_{7\pm}\rangle + i\epsilon|d_{xy}\rangle\chi_{\pm} + \eta(|d_{xz}\rangle \mp i|d_{yz}\rangle)\chi_{\mp}, \quad (\text{A}\cdot 4)$$

where ϵ , η and $\kappa = \sqrt{1 - \epsilon^2 - 2\eta^2}$ are real and χ_{\pm} describes the wave function of the spin. We note that the wave function of $|\Gamma_{7\pm}\rangle$ is given by

$$|\Gamma_{7\pm}\rangle = -\sqrt{\frac{5}{21}}i|L_z = 2-\rangle\chi_{\pm} \pm (\sqrt{\frac{15}{21}}|L_z = \pm 3\rangle - \sqrt{\frac{1}{21}}|L_z = \mp 1\rangle)\chi_{\mp}, \quad (\text{A}\cdot 5)$$

where $|L_z = 2-\rangle = \frac{1}{\sqrt{2i}}(|L_z = 2\rangle - |L_z = -2\rangle)$.

The periodical Anderson Hamiltonian is constructed for the localized $|f\pm\rangle$ state and conduction electrons. We here consider the conduction electrons arising from the Ce $5s$ -orbital for simplicity. Taking into account the inter-site hybridization between the s -, d - and f -orbitals, we obtain the tight-binding Hamiltonian

$$H_0 = \sum_{\vec{k}} \hat{\psi}_{\vec{k}}^{\dagger} \hat{H}_0(\vec{k}) \hat{\psi}_{\vec{k}}, \quad (\text{A}\cdot 6)$$

where $\hat{\psi}_{\vec{k}}^{\dagger} = (f_{\vec{k}+}^{\dagger}, f_{\vec{k}-}^{\dagger}, c_{\vec{k}\uparrow}^{\dagger}, c_{\vec{k}\downarrow}^{\dagger})$, and

$$\hat{H}_0(\vec{k}) = \begin{pmatrix} \hat{\epsilon}_f(\vec{k}) & \hat{V}(\vec{k}) \\ \hat{V}(\vec{k})^{\dagger} & \hat{\epsilon}_c(\vec{k}) \end{pmatrix}. \quad (\text{A}\cdot 7)$$

The 2×2 matrix $\hat{\epsilon}_f(\vec{k})$, $\hat{\epsilon}_c(\vec{k})$, and $\hat{V}(\vec{k})$ are obtained as

$$\hat{\epsilon}_f(\vec{k}) = \begin{pmatrix} \epsilon_f(\vec{k}) & \alpha_1(is_x + s_y) \\ \alpha_1(-is_x + s_y) & \epsilon_f(\vec{k}) \end{pmatrix}, \quad (\text{A}\cdot 8)$$

$$\hat{\epsilon}_c(\vec{k}) = \begin{pmatrix} \epsilon_c(\vec{k}) & 0 \\ 0 & \epsilon_c(\vec{k}) \end{pmatrix}, \quad (\text{A}\cdot 9)$$

$$\hat{V}(\vec{k}) =$$

$$\begin{pmatrix} (8V_3s_z + 4i\epsilon V_4)s_xs_y & (2iV_5 - 4\eta V_6s_z)(s_x + is_y) \\ (2iV_5 - 4\eta V_6s_z)(s_x - is_y) & (8V_3s_z + 4i\epsilon V_4)s_xs_y \end{pmatrix}, \quad (\text{A}\cdot 10)$$

where the abbreviation $s_{x,y,z} = \sin k_{x,y,z}$ is used. We ignored the off-diagonal terms in the second order with respect to the small parameters ϵ and η . We obtain $\epsilon_f(\vec{k}) = \kappa^2\epsilon_{\Gamma_7}(\vec{k}) + \epsilon^2\epsilon_{xy}(\vec{k}) + \eta^2(\epsilon_{xz}(\vec{k}) + \epsilon_{yz}(\vec{k}))$ where $\epsilon_A(\vec{k})$ is the dispersion relation for the $|A\rangle$ state. It is clearly shown that eq. (A.8) has the Rashba type spin-orbit coupling term and the coefficient is obtained as

$$\alpha_1 = -4\epsilon V_2 - 4\eta V_1. \quad (\text{A}\cdot 11)$$

The hybridization parameters in eqs. (A.10) and (A.11) are obtained as

$$V_1 = \kappa\sqrt{\frac{5}{21}}V_{2-,yz}^{100}, \quad (\text{A}\cdot 12)$$

$$V_2 = \kappa(\sqrt{\frac{15}{42}}V_{y^3-3x^2y,yz}^{100} - \sqrt{\frac{1}{42}}V_{y(5z^2-r^2),yz}^{100}), \quad (\text{A}\cdot 13)$$

$$V_3 = \kappa\sqrt{\frac{5}{21}}V_{2-,s}^{111}, \quad (\text{A}\cdot 14)$$

$$V_4 = V_{xy,s}^{110}, \quad (\text{A}\cdot 15)$$

$$V_5 = \kappa(\sqrt{\frac{15}{42}}V_{x^3-3xy^2,s}^{100} - \sqrt{\frac{1}{42}}V_{x(5z^2-r^2),s}^{100}), \quad (\text{A}\cdot 16)$$

$$V_6 = V_{xz,s}^{101}, \quad (\text{A}\cdot 17)$$

where $V_{A,B}^{abc}$ is the hopping matrix element between the $|A\rangle$ and $|B\rangle$ states along the $[abc]$ -axis.

Note that the parameters ϵ and η arise from the intra-site hybridization between the d - and f -orbitals while the matrix elements V_1 and V_2 describe the inter-site hybridization. Thus, the intra-orbital Rashba-type spin orbit coupling α_1 arises from the hybridization of the Γ_7 -state with the d_{xy} -, d_{xz} -, and d_{yz} -states. Note again that the parameters ϵ and η vanish in centrosymmetric systems.

Applying an appropriate unitary transformation to the conduction electron, $(c_{\vec{k}+}^{\dagger}, c_{\vec{k}-}^{\dagger}) = (c_{\vec{k}\uparrow}^{\dagger}, c_{\vec{k}\downarrow}^{\dagger})\hat{U}_c(\vec{k})$, the hybridization matrix is transformed as

$$\tilde{V}(\vec{k}) = \hat{V}(\vec{k})\hat{U}_c(\vec{k}) =$$

$$\begin{pmatrix} V_{cf}(\vec{k}) & \alpha_2(\vec{k})(is_y^2s_x + s_x^2s_y) \\ \alpha_2(\vec{k})(-is_y^2s_x + s_x^2s_y) & V_{cf}(\vec{k}) \end{pmatrix}, \quad (\text{A}\cdot 18)$$

where

$$\alpha_2(\vec{k}) = 4(\epsilon V_4 V_5 - 4\eta V_3 V_6 s_z^2) / \sqrt{16V_3^2 s_x^2 s_y^2 s_z^2 + V_5^2 (s_x^2 + s_y^2)}. \quad (\text{A}\cdot 19)$$

Note that $\alpha_2(\vec{k})$ is a real and even function with respect to k_x , k_y , and k_z .

Taking into account the on-site repulsion in the $|f\pm\rangle$ state, we obtain the periodical Anderson model with a Rashba-type ASOC as

$$H = H_k + H_{\text{ASOC}} + H_I, \quad (\text{A}\cdot 20)$$

$$H_k = \sum_{k,s=\pm} \varepsilon_f(\vec{k}) f_{k,s}^\dagger f_{k,s} + \sum_{k,s=\pm} \varepsilon_c(\vec{k}) c_{k,s}^\dagger c_{k,s} + \sum_{k,s=\pm} [V_{cf}(\vec{k}) f_{k,s}^\dagger c_{k,s} + h.c.], \quad (\text{A}\cdot 21)$$

$$H_{\text{ASOC}} = \alpha_1 \sum_{k,s,s'} \vec{g}_f(\vec{k}) \cdot \vec{\sigma}_{ss'} f_{k,s}^\dagger f_{k,s'} + \sum_{k,s,s'} [\alpha_2(\vec{k}) \vec{g}_{cf}(\vec{k}) \cdot \vec{\sigma}_{ss'} f_{k,s}^\dagger c_{k,s'} + h.c.], \quad (\text{A}\cdot 22)$$

$$H_I = U \sum_i n_{i,+}^f n_{i,-}^f, \quad (\text{A}\cdot 23)$$

where $\vec{g}_f(\vec{k}) = (\sin k_y, -\sin k_x, 0)$ and $\vec{g}_{cf}(\vec{k}) = (\sin^2 k_x \sin k_y, -\sin^2 k_x \sin k_x, 0)$ describe the g -vector for the intra- and inter-orbital Rashba-type ASOCs, respectively.

Note again that the ASOC arises from the atomic L - S coupling in the Ce $4f$ -orbital and the parity mixing in the localized state. The breakdown of the inversion symmetry plays an essential role in the parity mixing in the atomic state. The inter-site hybridization between the f - and admixed d -(or s -) orbitals gives rise to the intra-orbital ASOC, while the inter-orbital ASOC is induced by the hybridization between the conduction electrons and the admixed d - (or s -) orbitals. Note that the cubic term $\propto \sin k_x \sin k_y \sin k_z (\sin^2 k_x - \sin^2 k_y) \sigma_z$ ²⁶ does not appear in the above derivation.

We derived the periodical Anderson model for the localized $|\Gamma_6^\pm\rangle = |\pm \frac{1}{2}\rangle$ state and the conduction electrons with s -orbital symmetry. Then, we obtained the Hamiltonian that is similar to eq. (A.20), but the g -vector for the inter-orbital ASOC is replaced with $\vec{g}_{cf}(\vec{k}) = (\sin k_y, -\sin k_x, 0) = \vec{g}_f(\vec{k})$. Other crystal field levels different from eqs. (A.1)-(A.3) have been proposed.^{2,85} The Rashba-type ASOC can also be derived for these levels in the same way as above. Thus, the Rashba-type ASOC is generally derived in the periodical Anderson Hamiltonian by taking into account the parity mixing in the atomic $4f$ -state.

The kinetic energy term H_k in the periodical Anderson model is diagonalized by the unitary transformation $(a_{1,\vec{k}\pm}^\dagger, a_{2,\vec{k}\pm}^\dagger) = (f_{\vec{k}\pm}^\dagger, c_{\vec{k}\pm}^\dagger) \hat{U}_{cf}(\vec{k})$ with

$$\hat{U}_{cf}(\vec{k}) = \begin{pmatrix} a_1(\vec{k}) & a_2^*(\vec{k}) \\ a_2(\vec{k}) & -a_1(\vec{k}) \end{pmatrix}. \quad (\text{A}\cdot 24)$$

Applying this unitary transformation to the periodical Anderson model in eq. (A.20) and dropping the upper band described by $a_{2,\vec{k}\pm}^\dagger$, we obtain the single-orbital model with the Rashba-type ASOC. The g -vector is obtained as

$$\alpha \vec{g}(\vec{k}) = \alpha_1 a_1(\vec{k})^2 \vec{g}_f(\vec{k}) + \alpha_2(\vec{k}) a_1(\vec{k}) (a_2(\vec{k}) + a_2^*(\vec{k})) \vec{g}_{cf}(\vec{k}). \quad (\text{A}\cdot 25)$$

The unitary transformation described by $U_{cf}(\vec{k})$ leads to the momentum dependence of the two-body interaction term H_I , as in the case of the multi-orbital Hubbard model.⁸⁶ By neglecting this momentum dependence for simplicity, we obtain the single-orbital Hubbard model

in eq. (1) where the g -vector is described by eq. (A.25). The investigation of the periodical Anderson model in eq. (A.20) is an interesting future issue.

- 1) E. Bauer, G. Hilscher, H. Michor, Ch. Paul, E. W. Scheidt, A. Gribov, Yu. Seropegin, H. Noel, M. Sigrist, and P. Rogl: Phys. Rev. Lett **92** (2004) 027003.
- 2) E. Bauer, I. Bonalde, and M. Sigrist: J. Low. Temp. Phys. **31** (2005) 748; E. Bauer, H. Kaldarar, A. Prokofiev, E. Royanian, A. Amato, J. Sereni, W. Bramer-Escamilla, and I. Bonalde: J. Phys. Soc. Jpn. **76** (2007) 051009.
- 3) T. Akazawa, H. Hidaka, T. Fujiwara, T. C. Kobayashi, E. Yamamoto, Y. Haga, R. Settai, and Y. Onuki: J. Phys. Soc. Jpn. **73** (2004) 3129.
- 4) N. Kimura, K. Ito, K. Saitoh, Y. Umeda, and H. Aoki, and T. Terashima: Phys. Rev. Lett. **95** (2005) 247004.
- 5) N. Kimura, Y. Muro, and H. Aoki: J. Phys. Soc. Jpn. **76** (2007) 051010.
- 6) I. Sugitani, Y. Okuda, H. Shishido, T. Yamada, A. Thamizhavel, E. Yamamoto, T. D. Matsuda, Y. Haga, T. Takeuchi, R. Settai, and Y. Onuki: J. Phys. Soc. Jpn. **75** (2006) 043703.
- 7) R. Settai, T. Takeuchi, and Y. Onuki: J. Phys. Soc. Jpn. **76** (2007) 051003.
- 8) M. Measson, R. Settai and Y. Onuki: private communication; See also, A. Thamizhavel, H. Shishido, Y. Okuda, H. Harima, T. D. Matsuda, Y. Haga, R. Settai, and Y. Onuki: J. Phys. Soc. Jpn. **75** (2006) 044711.
- 9) K. Togano, P. Badica, Y. Nakamori, S. Orimo, H. Takeya, and K. Hirata: Phys. Rev. Lett. **93** (2004) 247004; P. Badica, T. Kondo, and K. Togano: J. Phys. Soc. Jpn. **74** (2005) 1014; See also, H. Q. Yuan, D. F. Agterberg, N. Hayashi, P. Badica, D. Vandervelde, K. Togano, M. Sigrist, and M. B. Salamon: Phys. Rev. Lett. **97** (2006) 017006; M. Nishiyama, Y. Inada, and G.-q. Zheng: Phys. Rev. Lett. **98** (2007) 047002.
- 10) C. Krupka, A. L. Giorgi, N. H. Krikorian, and E. G. Szklarz: J. Less Common Met. **19** (1969) 113; G. Amano, S. Akutagawa, T. Muranaka, Y. Zenitani, and J. Akimitsu: J. Phys. Soc. Jpn. **73** (2004) 530.
- 11) T. Shibayama, M. Nohara, H. Aruga Katori, Y. Okamoto, Z. Hiroi, and H. Takagi: J. Phys. Soc. Jpn. **76** (2007) 073708.
- 12) T. Klimczuk, Q. Xu, E. Morosan, J. D. Thompson, H. W. Zandbergen, and R. J. Cava: Phys. Rev. B **74** (2006) 220502(R); T. Klimczuk, F. Ronning, V. Sidorov, R. J. Cava, and J. D. Thompson: Phys. Rev. Lett. **99** (2007) 257004.
- 13) G. Mu, Y. Wang, L. Shan, and H.-H. Wen: Phys. Rev. B **76** (2007) 064527.
- 14) Y. L. Zuev, V. A. Kuznetsova, R. Prozorov, M. D. Vannette, M. V. Lobanov, D. K. Christen, and J. R. Thompson: Phys. Rev. B **76** (2007) 132508.
- 15) Z. Ren, J. Kato, T. Muranaka, J. Akimitsu, M. Kriener, and Y. Maeno: J. Phys. Soc. Jpn. **76** (2007) 103710.
- 16) E. Ohmichi: J. Superconductivity **12** (1999) 505.
- 17) V. M. Edelstein: Sov. Phys. JETP **68** (1989) 1244;
- 18) V. M. Edelstein: Phys. Rev. Lett **75** (1995) 2004; Phys. Rev. B **72** (2005) 172501.
- 19) S. K. Yip: Phys. Rev. B **65** (2002) 144508.
- 20) S. Fujimoto: Phys. Rev. B **74** (2005) 024515.
- 21) S. Fujimoto: J. Phys. Soc. Jpn. **76** (2007) 034712.
- 22) L. N. Bulaeviskii, A. A. Guseinov, and A. I. Rusinov: Sov. Phys. JETP **44** (1976) 1243.
- 23) L. P. Gor'kov and E. I. Rashba: Phys. Rev. Lett **87** (2001) 037004.
- 24) P. A. Frigeri, D. F. Agterberg, A. Koga, and M. Sigrist: Phys. Rev. Lett **92** (2004) 097001.
- 25) P. A. Frigeri, D. F. Agterberg, and M. Sigrist: New. J. Phys. **6** (2004) 115.
- 26) K. V. Samokhin: Phys. Rev. Lett **94** (2005) 027004.
- 27) V. P. Mineev and K. V. Samokhin: Phys. Rev. B **72** (2005) 212504.
- 28) Y. Yanase and M. Sigrist: J. Phys. Soc. Jpn. **76** (2007) 043712.
- 29) Y. Yanase and M. Sigrist: J. Phys. Soc. Jpn. **76** (2007) 124709.

- 30) N. Hayashi, K. Wakabayashi, P. A. Frigeri, and M. Sigrist: Phys. Rev. B **73** (2006) 092508.
- 31) S. Fujimoto: J. Phys. Soc. Jpn. **75** (2006) 083704.
- 32) N. Hayashi, K. Wakabayashi, P. A. Frigeri, and M. Sigrist: Phys. Rev. B **73** (2006) 024504.
- 33) I. Eremin and J. F. Annett: Phys. Rev. B **74** (2006) 184524.
- 34) V. P. Mineev and K. V. Samokhin; Zh. Eksp. Teor. Fiz. **105** (1994) 747 [Sov. Phys. JETP **78** (1994) 401].
- 35) O. V. Dimitrova and M. V. Feigel'man: JETP Lett. **78** (2003) 637; Phys. Rev. B **76** (2007) 014522.
- 36) K. V. Samokhin: Phys. Rev. B **70** (2004) 104521.
- 37) R. P. Kaur, D. F. Agterberg, and M. Sigrist: Phys. Rev. Lett. **94** (2005) 137002.
- 38) D. F. Agterberg and R. P. Kaur: Phys. Rev. B **75** (2007) 064511.
- 39) M. Oka, M. Ichioka, and K. Machida: Phys. Rev. B **73** (2006) 214509.
- 40) H. Tanaka, H. Kaneyasu, and Y. Hasegawa: J. Phys. Soc. Jpn. **76** (2007) 024715.
- 41) P. A. Frigeri, D. F. Agterberg, I. Milat, and M. Sigrist: cond-mat/0505108.
- 42) V. P. Mineev and K. V. Samokhin: Phys. Rev. B **75** (2007) 184529.
- 43) K. V. Samokhin: Phys. Rev. B **76** (2007) 094516.
- 44) B. Liu and I. Eremin: arXiv:0803.4514.
- 45) Y. Nagai, Y. Kato, and N. Hayashi: J. Phys. Soc. Jpn. **75** (2006) 043706.
- 46) Y. Matsunaga and R. Ikeda: arXiv:0801.0682.
- 47) I. A. Sergienko and C. H. Curnoe: Phys. Rev. B **70** (2004) 214510.
- 48) T. Yokoyama, Y. Tanaka, and J. Inoue: Phys. Rev. B **72** (2005) 220504.
- 49) K. Borkje and A. Sudbo: Phys. Rev. B **74** (2006) 054506.
- 50) B. Leridon, T.-K. Ng, and C. M. Varma: cond-mat/0604140.
- 51) C. Iniotakis, N. Hayashi, Y. Sawa, T. Yokoyama, U. May, Y. Tanaka, and M. Sigrist: Phys. Rev. B **76** (2007) 012501; C. Iniotakis, S. Fujimoto, and M. Sigrist: arXiv:0801.1373.
- 52) N. Hayashi: private communication.
- 53) Y. Tada, N. Kawakami, and S. Fujimoto: J. Phys. Soc. Jpn. **77** (2008) 054707.
- 54) T. Yokoyama, S. Onari, and Y. Tanaka: Phys. Rev. B **75** (2007) 172511.
- 55) A. Amato, E. Bauer, and C. Baines: Phys. Rev. B **71** (2005) 092501.
- 56) M. Yogi, Y. Kitaoka, S. Hashimoto, T. Yasuda, R. Settai, T. D. Matsuda, Y. Haga, Y. Onuki, P. Rogl, and E. Bauer: Phys. Rev. Lett. **93** (2004) 027003.
- 57) N. Metoki, K. Kaneko, T. D. Matsuda, A. Galatanu, T. Takeuchi, S. Hashimoto, T. Ueda, R. Settai, Y. Onuki, and N. Bernhoeft: J. Phys. Condens. Matter **16** (2004) L207.
- 58) T. Yasuda, H. Shishido, T. Ueda, S. Hashimoto, R. Settai, T. Takeuchi, T. D. Matsuda, Y. Haga, and Y. Onuki: J. Phys. Soc. Jpn. **73** (2004) 1657.
- 59) T. Tateiwa, Y. Haga, T. D. Matsuda, S. Ikeda, T. Yasuda, T. Takeuchi, R. Settai, and Y. Onuki: J. Phys. Soc. Jpn. **74** (2005) 1903.
- 60) T. Takeuchi, M. Shiimoto, H. Kohara, T. Yasuda, S. Hashimoto, R. Settai, and Y. Onuki: Physica B **378-80** (2006) 376.
- 61) K. Izawa, Y. Kasahara, Y. Matsuda, K. Behnia, T. Yasuda, R. Settai, and Y. Onuki: Phys. Rev. Lett. **94** (2005) 197002.
- 62) I. Bonalde, W. Bramer-Escamilla, and E. Bauer: Phys. Rev. Lett. **94** (2005) 207002.
- 63) T. Takeuchi, T. Yasuda, M. Tsujino, H. Shishido, R. Settai, H. Harima, and Y. Onuki: J. Phys. Soc. Jpn. **76** (2007) 014702.
- 64) H. Mukuda, S. Nishide, A. Harada, K. Iwasaki, M. Yogi, M. Yashima, Y. Kitaoka, M. Tsujino, T. Takeuchi, R. Settai, Y. Onuki, E. Bauer, K. M. Itoh, and E. E. Haller: preprint.
- 65) M. Yogi, H. Mukuda, Y. Kitaoka, S. Hashimoto, T. Yasuda, R. Settai, T. D. Matsuda, Y. Haga, Y. Onuki, P. Rogl, and E. Bauer: J. Phys. Soc. Jpn. **75** (2006) 013709.
- 66) W. Higemoto, Y. Haga, T. D. Matsuda, Y. Onuki, K. Ohishi, T. U. Ito, A. Koda, S. R. Saha, and R. Kadono: J. Phys. Soc. Jpn. **75** (2006) 124713.
- 67) Y. Yanase, T. Jujo, T. Nomura, H. Ikeda, T. Hotta, and K. Yamada: Phys. Rep. **387** (2004) 1.
- 68) A. Kozhevnikov and V. Ansimov: private communication.
- 69) K. V. Samokhin, E. S. Zijlstra, and S. K. Bose: Phys. Rev. B **69** (2004) 094514.
- 70) S. Hashimoto, T. Yasuda, T. Kubo, H. Shishido, T. Ueda, R. Settai, T. D. Matsuda, Y. Haga, H. Harima, and Y. Onuki: J. Phys. Condens. Matter **16** (2004) L287.
- 71) E. I. Rashba: Sov. Phys. Solid State **1** (1959) 368.
- 72) For a review, Y. Kitaoka, S. Kawasaki, T. Mito, and Y. Kawasaki: J. Phys. Soc. Jpn. **74** (2005) 186; J. Flouquet, G. Knebel, D. Braithwaite, D. Aoki, J. P. Brison, F. Hardy, A. Huxley, S. Raymond, B. Salce, and I. Sheikin: cond-mat/0505713.
- 73) K. Miyake, S. Schmitt-Rink, and C. M. Varma: Phys. Rev. B **34** (1986) 6554; D. J. Scalapino, E. Loh Jr., and J. E. Hirsch: Phys. Rev. B **34** (1986) 8190.
- 74) K. Machida: J. Phys. Soc. Jpn. **50** (1981) 2195; G. C. Psaltakis and E. W. Fenton: J. Phys. C **16** (1983) 3913; M. Kato and K. Machida: Phys. Rev. B **37** (1988) 1510; M. Murakami and H. Fukuyama: J. Phys. Soc. Jpn. **67** (1998) 2784; B. Kyung: Phys. Rev. B **62** (2000) 9083; A. Aperis, G. Varelogiannis, P. B. Littlewood, and B. D. Simon: arXiv: 0804.2460.
- 75) C. Pfleiderer, D. Reznik, L. Pintschovius, H. v. Lohneysen, M. Garst, and A. Rosch: Nature **427** (2004) 227.
- 76) A. J. Leggett: Rev. Mod. Phys. **47** (1975) 331.
- 77) M. Sigrist and K. Ueda: Rev. Mod. Phys. **63** (1991) 239.
- 78) H. Shimahara: Phys. Rev. B **72** (2005) 134518.
- 79) T. Nomura and K. Yamada: J. Phys. Soc. Jpn. **71** (2002) 404.
- 80) Y. Yanase, M. Mochizuki, and M. Ogata: J. Phys. Soc. Jpn. **74** (2005) 3351.
- 81) K. Nakatsuji, A. Sumiyama, Y. Oda, T. Yasuda, R. Settai, and Y. Onuki: J. Phys. Soc. Jpn. **75** (2006) 084717.
- 82) Y. Aoki, A. Sumiyama, G. Motoyama, Y. Oda, T. Yasuda, R. Settai, and Y. Onuki: J. Phys. Soc. Jpn. **76** (2007) 114708.
- 83) G. Motoyama, K. Maeda and Y. Oda: J. Phys. Soc. Jpn. **77** (2008) 044710.
- 84) The coefficients in $|\Gamma_{7\pm}\rangle$ and $|\Gamma'_{7\pm}\rangle$ are slightly different from those reported in ref. 57, but the difference is not important in the following discussion.
- 85) G. Motoyama: private communication.
- 86) Y. Yanase, M. Mochizuki, and M. Ogata: J. Phys. Soc. Jpn. **74** (2005) 430.